

Mechanism of Inner-Sphere Electron Transfer via Charge-Transfer (Precursor) Complexes. Redox Energetics of Aromatic Donors with the Nitrosonium Acceptor

Sergiy V. Rosokha and Jay K. Kochi*

Contribution from the Department of Chemistry, University of Houston, Houston, Texas 77204-5641

Received April 2, 2001. Revised Manuscript Received June 25, 2001

Abstract: Spontaneous formation of colored (1:1) complexes of various aromatic donors (**ArH**) with the nitrosonium acceptor (NO^+) is accompanied by the appearance of two new (charge-transfer) absorption bands in the UV–vis spectrum. IR spectral and X-ray crystallographic analyses of the $[\text{ArH}, \text{NO}^+]$ complexes reveal their inner-sphere character by the **ArH**/ NO^+ separation that is substantially less than the van der Waals contact and by the significant enlargement of the aromatic chromophore. The reversible interchange between such an inner-sphere complex $[\text{ArH}, \text{NO}^+]$ and the redox product ($\text{ArH}^{\bullet+} + \text{NO}^\bullet$) is quantitatively assessed for the first time to establish it as the critical intermediate in the overall electron-transfer process. Theoretical formulation of the NO^+ binding to **ArH** is examined by LCAO-MO methodology sufficient to allow the unambiguous assignment of the pair of diagnostic (UV–vis) spectral bands. The MO treatment also provides quantitative insight into the high degree of charge-transfer extant in these inner-sphere complexes as a function of the HOMO–LUMO gap for the donor/acceptor pair. The relative stabilization of $[\text{ArH}, \text{NO}^+]$ is traced directly to the variation in the electronic coupling element H_{AB} , which is found to be substantially larger than the reorganization energy ($\lambda/2$). In Sutin's development of Marcus–Hush theory, this inequality characterizes a completely delocalized *Class III* complex (which occupies a single potential well) according to the Robin–Day classification. The mechanistic relevance of such an unusual (precursor) complex to the inner-sphere mechanism for organic electron transfer is discussed.

Introduction

Electron transfer from organic donors (particularly to large inorganic oxidants) is theoretically well-accommodated by the Marcus (outer-sphere) formalism that derives from weakly bonded ($<200 \text{ cm}^{-1}$) transition states.^{1,2} However, in the more general situation encountered with most of the common organic (redox) processes, the electronic interaction in the transition state can be substantial ($>1000 \text{ cm}^{-1}$),^{1,3,4} and this mechanistic ambiguity is apparent in the ubiquitous formation of (preequilibrium) charge-transfer complexes,⁵ the *inner-sphere* character of which is established by their high sensitivity to steric effects.⁶

As common as charge-transfer complexes are, it has never been directly established that they are the immediate (inner-sphere) precursor to the transition states for the electron-transfer process itself.⁷ Since part of this void is attributable to the dearth of organic donors (**D**) that afford persistent cation radicals ($\text{D}^{\bullet+}$),

we focus our attention on two classes of aromatic donors (**ArH**) with the graded series of oxidation potentials (E°_{ox}) listed in Chart 1.

The aromatic donors in **Class I** consist of (homologous) methylbenzenes with donor strengths that encompass a 25 kcal mol⁻¹ range, progressively decreasing from hexamethylbenzene to benzene.⁸ The **Class II** arenes are significantly more electron-rich, with enhanced donor strengths in the lower range: $1.16 \text{ V} < E^\circ_{\text{ox}} < 1.45 \text{ V}$.⁹ Most notably, the sterically encumbered arene donors in **Class II** are readily oxidized to cation radicals ($\text{ArH}^{\bullet+}$) that are sufficiently persistent to allow their isolation as crystalline salts amenable to direct X-ray crystallographic (structure) analysis. By comparison, the poorer arene donors in **Class I** suffer one-electron oxidation to cation radicals ($\text{ArH}^{\bullet+}$) that for the most part are highly transient species (even **HMB**^{•+} from the hexamethylbenzene donor with $E^\circ_{\text{ox}} = 1.62 \text{ V}$) and elude isolation as crystalline salts.

For the oxidant component, we chose the nitrosonium cation (NO^+), owing to its acceptor strength $E^\circ_{\text{red}} = 1.48 \text{ V}$ that lies at the border between **Class I** and **Class II** donors.¹⁰ In other words, the driving force [$\Delta G^\circ_{\text{ET}} = \mathcal{F}(E^\circ_{\text{ox}} - E^\circ_{\text{red}})$] for

(1) (a) Ebersson, L. *Electron Transfer Reactions in Organic Chemistry*; Springer-Verlag: New York, 1987. (b) Piotrowiak, P., Ed. *Principles and Theories*; Vol. 1, Part 1 in *Electron Transfer in Chemistry*; Balzani V., Ed.; Wiley-VCH: Weinheim, 2001.

(2) Astruc, D. *Electron Transfer and Radical Processes in Transition-Metal Chemistry*; VCH: New York, 1995. (b) Mattay, J., Ed. *Organic Molecules*; Vol. 2, Part 1 in *Electron Transfer in Chemistry*; Balzani V., Ed.; Wiley-VCH: Weinheim, 2001.

(3) Ebersson, L.; Shaik, S. S. *J. Am. Chem. Soc.* **1990**, *112*, 4484.

(4) (a) Hubig, S. M.; Rathore, R.; Kochi, J. K. *J. Am. Chem. Soc.* **1999**, *121*, 617. (b) Hubig, S. M.; Kochi, J. K. *J. Am. Chem. Soc.* **1999**, *121*, 1688. (c) Rathore, R.; Hubig, S. M.; Kochi, J. K. *J. Am. Chem. Soc.* **1997**, *119*, 11468.

(5) (a) Foster, R. *Organic Charge-Transfer Complexes*; Academic: New York, 1969. (b) Briegleb, G. *Electronen-Donator-Acceptor Komplexe*; Springer: Berlin, 1961.

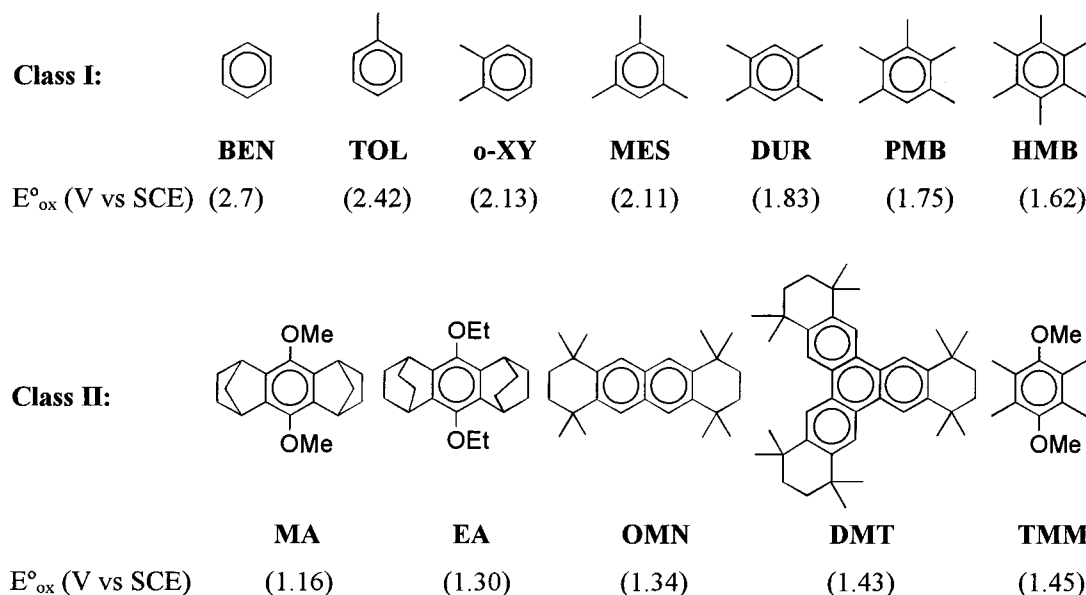
(6) Rathore, R.; Lindeman, S.; Kochi, J. K. *J. Am. Chem. Soc.* **1997**, *119*, 9393.

(7) Compare: Colter, A. K.; Dack, M. R. J. In *Molecular Complexes*; Foster, R., Ed.; Crane Russak: New York, 1974; Vol. 2, p 1 for the mechanistic ambiguity.

(8) (a) Howell, J. O.; Goncalves, J. M.; Amatore, C.; Klasinc, L.; Wightman, R. M.; Kochi, J. K. *J. Am. Chem. Soc.* **1984**, *106*, 3968. (b) For the definition of donor strength in the context of E°_{ox} , see: Kochi, J. K. *Comprehensive Organic Synthesis*; Trost, B., Fleming, I., Eds., Elsevier: New York, 1991, Vol. 1.

(9) (a) Rathore, R.; Kumar, A. S.; Lindeman, S.; Kochi, J. K. *J. Org. Chem.* **1998**, *63*, 5847. (b) Rathore, R.; Kochi, J. K. *Can. J. Chem.* **1998**, *77*, 913. (c) E°_{ox} for **DMT** and **TMM** are reported in the Experimental Section.

Chart 1



reversible electron transfer as in eq 1 is essentially nil for



hexamethylbenzene and hydroquinone ether (see **HMB** and **TMM** in Chart 1). As such, the (electron-transfer) driving force becomes increasingly more endergonic and exergonic as we proceed further into the series of **Class I** and **Class II** donors, respectively. Furthermore, the use of the diatomic NO^+ oxidant allows the electronic properties of various (1:1) arene complexes to be quantitatively probed since there is a large change in the simple IR stretching frequency (ν_{NO}) upon its conversion to the reduced nitric oxide (NO^\bullet). In this study, we describe how the observation and characterization of various $[\text{ArH}, \text{NO}^+]$ species as preequilibrium (precursor) intermediates in eq 1 play a critical role in elucidating the mechanism of inner-sphere electron transfer for different arenes as a prototypical class of organic donors.

Results

I. Spontaneous Complexation of (Class I) Aromatic Donors with Nitrosonium Cation. A. Spectral (UV-vis) Appearance of New Absorption Bands and the Spontaneous Formation of Charge-Transfer Complexes. The exposure of aromatic donors in **Class I** to NO^+ (at room temperature) resulted immediately in a distinctive yellow to red coloration of the dichloromethane solution.¹¹ UV-vis analysis of the brightly colored solutions uniformly revealed a pair of new absorption bands: an intense high-energy band (H) with $\lambda_{\text{max}} \approx 340$ nm and a weak broad band (L) centered near 500 nm. Figure 1A and B illustrates how the partially resolved (overlapping) bands were deconvoluted into a pair of Gaussian components, and the absorption maxima of spectral bands H and L are compiled in Table 1. Most importantly, the linear correlation of the low-energy bands ($h\nu_{\text{L}}$) with the oxidation

potential (E°_{ox}) of **Class I** donors in Figure 1C was highly diagnostic of charge-transfer transitions of the type predicted by Mulliken.¹²

B. Formation Constant of Arene/ NO^+ Complexes. For relatively weak donors (benzene to mesitylene), quantitative spectral analysis with changes in **ArH** and NO^+ concentrations (from 0.05 to 20 and 0.2 to 2.0 mM, respectively) indicated that the absorbance increase was solely determined by the 1:1 formation of electron donor/acceptor complexes, which we designate hereafter as charge-transfer (CT) complexes.



Treatment of the absorption data for the intense band H by either the Benesi-Hildebrand procedure¹³ or the graphical method of Drago¹⁴ yielded the formation constants (K_{CT}) and the extinction coefficients (ϵ_{CT}) listed in Table 1.

For the stronger donors (durene to hexamethylbenzene), the absorbance change with increasing **ArH** concentration (NO^+ in excess) was quite linear, and ϵ_{CT} was evaluated directly from the (practically) complete complexation, i.e., $[\text{ArH}, \text{NO}^+] = [\text{ArH}]_0$ (see Experimental Section for details). The sizable formation constant obtained in this manner underscored the large variation in the formation constant with donor strength (with K_{CT} increasing by a factor of 10^5 from benzene to hexamethylbenzene) that is expected from an important charge-transfer component in the electron donor/acceptor complex.⁵

C. Molecular Structure of Arene/ NO^+ Complexes. The slow diffusion of hexane into highly colored solutions of **Class I** arenes and NO^+ in dichloromethane afforded crystalline salts of the general structure depicted in Chart 2, in which X-ray crystallographic analysis reveals the noncovalently bound NO to lie directly above the aromatic ring.

Moreover, the inner-sphere character of the $[\text{ArH}, \text{NO}^+]$ complex is established by the intermolecular separation of ~ 2.1 Å, which is significantly closer than the sum of the van der

(10) (a) Lee, K. Y.; Kuchynka, D. J.; Kochi, J. K. *Inorg. Chem.* **1990**, 29, 4196. (b) Nitrosonium was generally used as hexachloroantimonate salt. For convenience, the SbCl_6^- counterion will be omitted hereinafter.

(11) (a) Kim, E. K.; Kochi, J. K. *J. Am. Chem. Soc.* **1991**, 113, 4962. (b) Note that $h\nu_{\text{H}}$ and $h\nu_{\text{L}}$ in dichloromethane are essentially the same as those reported in acetonitrile. However, the values of K_{CT} in dichloromethane are an order of magnitude larger than those in acetonitrile owing to enhanced (ionic) solvation.

(12) (a) Mulliken, R. S. *J. Am. Chem. Soc.* **1952**, 74, 811. (b) Mulliken, R. S.; Person, W. B. *Molecular Complexes*; Wiley: New York, 1969.

(13) Benesi, H. A.; Hildebrand, J. H. *J. Am. Chem. Soc.* **1949**, 71, 2703.

(14) (a) Drago, R. S. *Physical Methods in Chemistry*; W. B. Saunders Company: Philadelphia, 1977. (b) Rose, N. J.; Drago, R. S. *J. Am. Chem. Soc.* **1959**, 81, 6138.

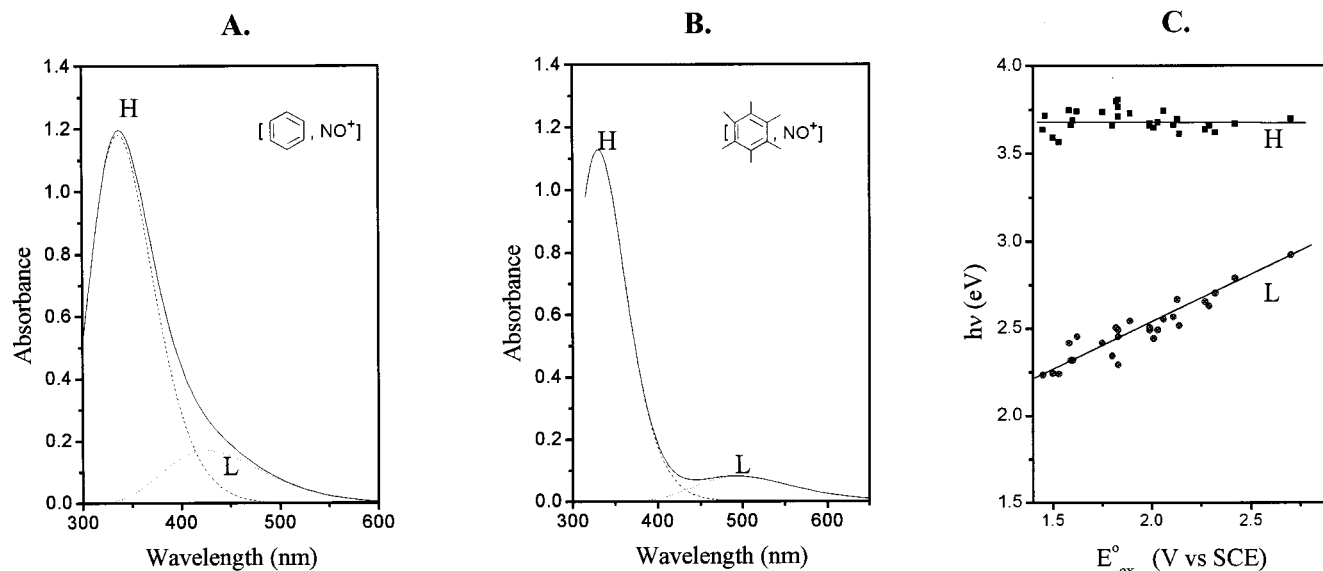
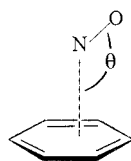


Figure 1. Charge-transfer spectrum of the NO^+ complexes with (A) benzene and (B) hexamethylbenzene showing the Gaussian deconvolution of the high-energy (H) and low-energy (L) absorption bands. (C) Mulliken plots of the H and L bands for the (Class I) aromatic donors identified in Tables 1 and S4.

Chart 2



Waals radii of 3.25 \AA .¹⁵ An oblique (bent) orientation with $\theta \approx 140 \pm 10^\circ$ is optimum for most of the arene/ NO^+ associations, as described in Tables 2 and S1 (see Supplementary Information). Most importantly, the complexation of NO^+ can lead to an (average) expansion of the aromatic (C–C) bond length of $\Delta = 1.1 \pm 0.3 \text{ pm}$ to approach that of the (oxidized) aromatic cation radical, as well as the lengthening of the N–O bond close to that of the reduced nitric oxide (1.15 \AA) rather than that of the uncomplexed N–O^+ (1.06 \AA). The latter was independently confirmed by measurements of the IR stretching frequency (ν_{NO} Table 1), which approximates that of nitric oxide (1876 cm^{-1}) rather than that of free NO^+ (2272 cm^{-1}),¹¹ especially in complexes with strong donors such as **HMB** and **PMB**. Thus the X-ray and IR data are consistent and show that NO^+ complexes with strong Class I donors essentially represent the close association of the oxidized arene with nitric oxide.

D. Thermal Stability of Arene/ NO^+ Complexes. Most alkylbenzene complexes with NO^+ were relatively persistent in dichloromethane (at room temperature) if carefully protected from air, moisture, and light. However, upon prolonged standing, the absorbance of the highly colored solution gradually diminished as nitric oxide evolved slowly. The effect was most pronounced with the electron-rich donors, such as penta- and hexamethylbenzene. Furthermore, in the case of the electron-rich difunctional donor octamethyl(diphenyl)methane **ODM** (see Table 1), the initially formed [arene, NO^+] complex (with coloration similar to those of **HMB** and **PMB**) changed dramatically over 2 h, as illustrated in Figure 2A. Spectrophotometric analysis (together with the X-ray structure determination of the cationic product crystallized from solution) indicated a facile first-order (oxidative) transformation (Figure 2B) of the arene component to its cation via an initial (intracomplex)

electron transfer.¹⁶ To pursue this conclusion further, we next turned to the Class II aromatic donors since they produce persistent cation radicals that are amenable to *direct* analysis in the following way.

II. Spectral and Structural Characterization of Oxidized (Class II) Aromatic Donors. A. Distinctive UV–vis Spectra of (Persistent) Aromatic Cation Radicals. Class II aromatic donors were subject to rapid oxidation with chemical oxidants such as SbCl_5 and $\text{Et}_3\text{O}^+\text{SbCl}_6^-$ at 25°C and afforded quantitative yields of persistent cation radicals ($\text{ArH}^{+\bullet}$) in dichloromethane solution.⁹ Similarly, anodic coulometry of these aromatic donors in dichloromethane solutions (containing 0.1 M tetrabutylammonium hexachloroantimonate as supporting electrolyte) confirmed the facile (one-electron) transformation:¹⁷



The highly colored (orange) solutions of the cation radicals from the hydroquinone ethers (see **MA**, **EA**, and **TMM** in Chart 1) were characterized by an intense absorption band at $\lambda_{\text{max}} \approx 500 \text{ nm}$ (Figure 3A) with a extinction coefficient of $4000\text{--}8000 \text{ M}^{-1}\text{cm}^{-1}$ (Table 3). Moreover, the polycyclic hydrocarbon donors **OMN** and **DMT** (identified in Chart 1) also afforded stable solutions of highly colored (red) cation radicals showing slightly shifted absorption bands (with resolved vibrational fine structure) at $\lambda_{\text{max}} = 700\text{--}750 \text{ nm}$ and $\epsilon_{\text{max}} = 8600 \text{ M}^{-1}\text{cm}^{-1}$ (**OMN**) and $25\,000 \text{ M}^{-1}\text{cm}^{-1}$ (**DMT**) (see Table 3).

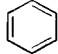
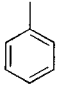
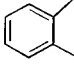

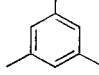
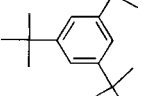
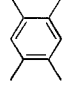
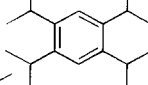
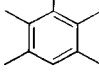
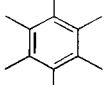
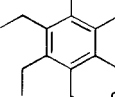
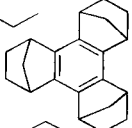
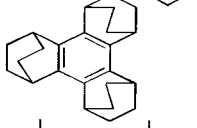
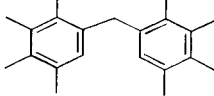
B. X-ray Crystallographic Analysis of Persistent Aromatic Cation Radicals and Structural Comparison with Neutral Donors. The successful isolation of single crystals of the cation-

(16) In Figure 2, the first-order decrease of the absorbance at $\lambda_{\text{max}} = 340 \text{ nm}$ with $k_1 = 5.9 \times 10^{-4} \text{ s}^{-1}$ was the same as the absorbance growth at $\lambda_{\text{max}} = 515 \text{ nm}$ with $k_1 = 5.5 \times 10^{-4} \text{ s}^{-1}$. The 340-nm band corresponds to $h\nu_{\text{H}}$ of the [ODM, NO^+] complex, and the 515-nm band is due to the diarylmethyl cation $[(\text{CH}_3)_4\text{C}_6\text{H}]_2\text{CH}^+$, which has been isolated as the SbCl_6^- salt; the X-ray crystallographic structure is presented in the Supporting Information. The facile production of this cation from **ODM**⁺ occurs via rapid proton loss and oxidation of the resultant radical; see: Schlesener, C. J.; Amatore, C.; Kochi, J. K. *J. Am. Chem. Soc.* **1984**, *106*, 7472. Rollick, K. L.; Kochi, J. K. *J. Org. Chem.* **1982**, *47*, 435.

(17) Compare also: Rathore, R.; Lindeman, S.; Kumar, A. S.; Kochi, J. K. *J. Am. Chem. Soc.* **1998**, *120*, 6931.

(15) Bondi, A. *J. Phys. Chem.* **1964**, *68*, 441.

Table 1. Spectral Characteristics and Formation Constants of $[\text{ArH},\text{NO}^+]$ Complexes for **Class I** Donors^a

	Aromatic donor	E_{ox}^0 (V vs SCE) ^b	λ_{H} (nm) [$10^{-3}\epsilon$, $\text{M}^{-1}\text{cm}^{-1}$]	λ_{L} (nm)	K_{CT} (M^{-1})	ν_{NO}^c (cm^{-1})
1	BEN 	2.7	336 [1.6]	425	6.0×10^0	2075
2	TOL 	2.42	338 [3.5]	445	3.5×10^1	2030
3	o-XY 	2.13	336 [3.6]	466	2.5×10^2	2000
4	p-XY 	2.06	332 [4.0]	486	3.0×10^2	1998
5	MES 	2.11	339 [5.8]	484	2.0×10^3	1964
6	TBB 	2.01	340 [5.0]	508	4.1×10^3	1964
7	DUR 	1.83	330 [7.0]	506	1.5×10^4	1933
8	TPB 	1.81	339 [6.8]	530	1.4×10^2	d)
9	PMB 	1.75	332 [8.2]	513	2.9×10^5	1907
10	HMB 	1.62	332 [8.0]	507	6.0×10^5	1885
11	HEB 	1.59	339 [7.9]	535	4.1×10^5	1900
12	TMT 	1.50	346 [6.6]	553	3.2×10^5	1910
13	TET 	1.55	347 [7.7]	553	d)	1890
14	ODM 	1.70	330 [d]	512	d)	d)

^a In CH_2Cl_2 , at 22 °C. ^b Entries 1–11 from refs 1a and 11. ^c Entries 1–11 from ref 11. ^d Not measured.

Table 2. Selected Bond Lengths, Bond Angles and Distances for the $[\text{ArH},\text{NO}^+]$ Complexes of **Class I** Donors^a

donor	$l^{b,c}$	$d_c^{b,d}$	θ^e	$d_{\text{NO}}^{b,f}$	$\bar{d}_{\text{CC}}^{b,g}$	\bar{d} (donor) ^{b,h}
o-XY	2.192	0.312	153	1.080	1.400	
p-XY	2.155	0.261	157	1.084	1.398	1.392
DUR	2.092	0.268	138	1.093	1.401	
PMB	2.049	0.495	131	1.110	1.398	

^a For data for nitrosonium complexes with **MES**,¹¹ **HMB**,²² **HEB**,⁶ **TET**⁶ and **TMT**²² see Table S1 in Supplementary Information. ^b In angstroms. ^c Distance from N to arene plane. ^d Distance of the perpendicular from N to the ring center. ^e Angle (in degrees) between NO axis and the normal to the arene plane. ^f N–O bond length. ^g Average C–C distance of the donor moiety in $[\text{ArH},\text{NO}^+]$. ^h Average C–C distance in the uncomplexed donor.

radical salts $\text{ArH}^+\text{SbCl}_6^-$ from the hydroquinone donors ($\text{ArH} = \text{MA}$ and EA) and the naphthalene donor **OMN** allowed the accurate determination of the relevant C–C bond lengths in the aromatic chromophores. For comparison, Tables 4 and S2 also list the corresponding C–C bond lengths in their neutral precursor (ArH). In each case, the aromatic C–C bond lengths in ArH suffered significant changes upon one-electron oxidation

to ArH^+ ,¹⁸ and the increase in the average bond length of ~ 2 pm for MA/MA^+ and EA/EA^+ and 0.4 pm for OMN/OMN^+ (Tables 4 and S2) was consistent with the expansion of the aromatic chromophore owing to the decreased bond orders following one-electron oxidation, as predicted by Pauling.¹⁹ Furthermore, the extensive charge delocalization in aromatic cation radicals is shown in the structure of MA^+ and EA^+ by the coplanarization of the pair of alkoxy substituents, as measured by the large decrease in the dihedral angle β (Tables 4 and S2) upon one-electron oxidation.²⁰

III. Spontaneous Complexation and Electron Transfer of Class II Aromatic Donors with Nitrosonium Cation. A. Spectral Identification of $[\text{ArH},\text{NO}^+]$ Complexes and ArH^+ Cation Radicals. Exposure of the **Class II** arenes to a colorless solution of NO^+ at -40 °C rapidly led to the bright greenish

(18) (a) Hubig, S. M.; Lindeman, S.; Kochi, J. K. *Coord. Chem. Rev.* **2000**, *200*, 831. (b) Kochi, J. K. Rathore, R.; LeMagueres, P. *J. Org. Chem.* **2000**, *21*, 6826.

(19) Pauling, L. *The Nature of the Chemical Bond*. Cornell University Press: Ithaca, NY, 1960; pp 255–256.

(20) Rathore, R.; Kochi, J. K. *J. Org. Chem.* **1995**, *60*, 4399.

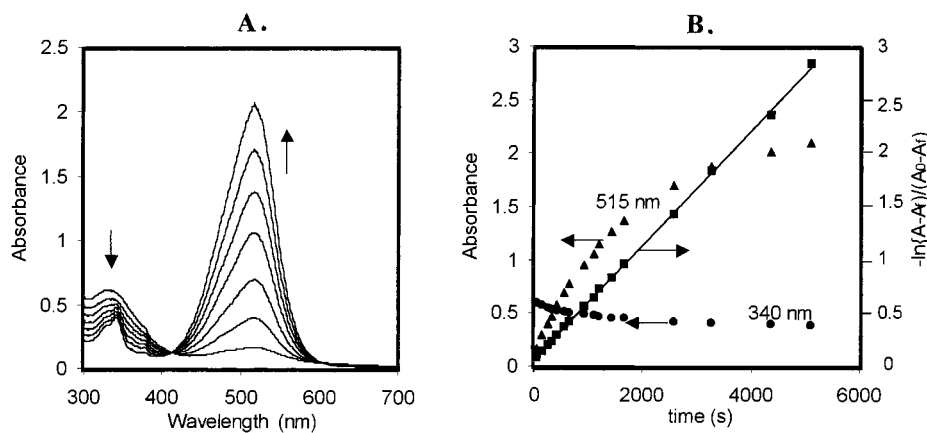


Figure 2. (A) Spectral change accompanying the oxidation of ODM by $\text{NO}^+\text{SbCl}_6^-$ in dichloromethane at 22 °C showing the diminution of the high-energy band of the $[\text{ODM},\text{NO}^+]$ complex and the growth the diarylmethyl cation with $\lambda_{\text{max}} = 515$ nm. (B) Kinetics of the 340-nm and 515-nm bands (left scale), together with the first-order kinetics treatment (right scale).

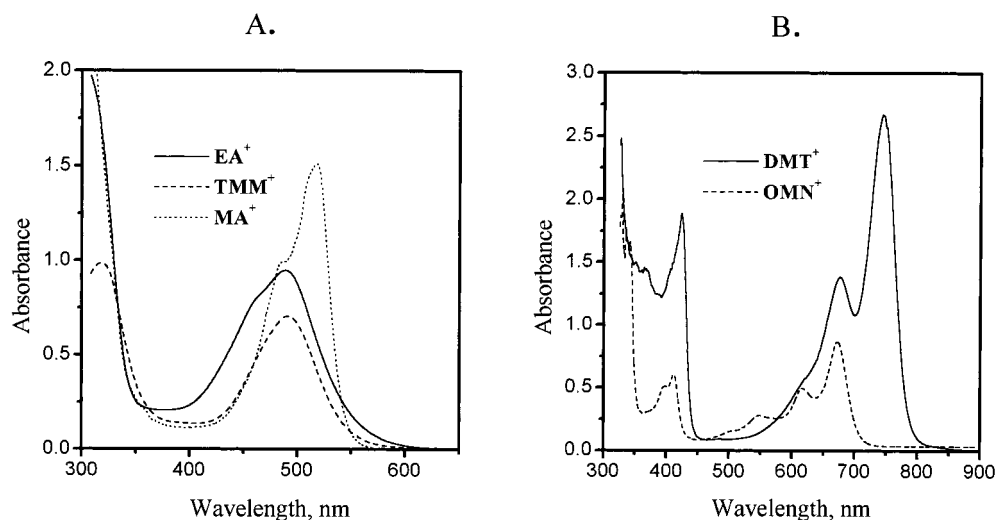


Figure 3. Absorption spectra of the cation radicals of (Class II) aromatic donors in dichloromethane: (A) benzenoid donors and (B) polynuclear donors (as indicated) at approximately the same concentrations ($\sim 10^{-4}$ M).

Table 3. Spectral Characteristics of Class II Cation Radicals^a

donor	λ , nm ($10^{-3}\epsilon$, $\text{M}^{-1}\text{cm}^{-1}$)
15 MA ^c	486 sh ^b ; 518 (8.3)
16 EA	463 sh; 492 (4.8)
17 OMN ^c	396 (5.0); 412 (5.9); 547 (2.6); 617 (4.8); 672 (8.6)
18 DMT	405 sh; 423 (17); 619 sh; 675 (12); 745 (25)
19 TMM	460 sh; 492 (3.5)

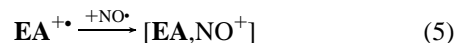
^a In dichloromethane solution, principal bands in bold. ^b Shoulder. ^c Reference 9.

coloration of the dichloromethane solution (somewhat reminiscent of the color changes observed with Class I donors), but the liberation of some nitric oxide from solution was immediately apparent from the IR spectrum ($\nu_{\text{NO}} = 1876\text{ cm}^{-1}$) of a gas sample. In harmony with this observation, UV-vis analysis of a mixture of hydroquinone donor EA and NO^+ revealed a composite spectrum consisting of the overlapping bands of the $[\text{EA},\text{NO}^+]$ complex with its principal absorption at $\lambda_{\text{max}} = 348$ nm (compare the charge-transfer spectra in Figure 1/Table 1), as well as the characteristic absorption bands of the cation radical $\text{EA}^{+\bullet}$ with $\lambda_{\text{max}} = 492$ nm (Table 3).^{20,21} The complete removal of the NO^{\bullet} gas in vacuo (or by entrainment with argon) resulted in the clear orange solution showing a simplified spectrum (Figure 4A), consisting of only the diag-

nostic bands of cation-radical, i.e.,

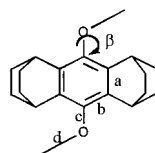


Likewise, the reintroduction of (1 equiv) NO^{\bullet} regenerated the original (composite) solution, and the further addition of NO^{\bullet} (excess) led to the clean green solution consisting of only the charge-transfer spectrum (Figure 4A) with an intense band at $\lambda_{\text{max}} = 348$ nm ($\epsilon_{348} = 7100\text{ M}^{-1}\text{cm}^{-1}$) together with a weak, broad band centered at $\lambda_{\text{max}} = 590$ nm, i.e.,



Identical series of color and spectral changes were independently observed when a crystalline sample of the pure salt $\text{EA}^{+\bullet}\text{SbCl}_6^-$ was treated with NO^{\bullet} in dichloromethane solution. The series of spectral changes associated with eqs 4 and 5 could be repeated indefinitely with no degradation of the absorbances.

The other aromatic donors in Class II upon the addition of NO^+ showed the same propensity to simultaneously form the charge-transfer complex and the aromatic cation-radical, the relative amounts of which were readily modulated by the removal/addition of nitric oxide. The spectral properties of the $[\text{ArH},\text{NO}^+]$ complexes in Table 5 show the same general features as the charge-transfer complexes derived from Class I

Table 4. Selected Bond Lengths^a and Angles^b for **Class II** Donor **EA**, Its Cation Radicals **EA⁺** and **[EA,NO]⁺** Complexes^c

donor	l^d	θ^d	d_{NO}^d	a	b	c	d	\bar{d}_{CC}^e	β^f	Δ^g
EA				1.407	1.399	1.399	1.441	1.401	87.4	
EA⁺				1.383	1.435	1.328	1.459	1.418	19.7	0.017
[EA,NO]⁺	2.089	127.5	1.126	1.403	1.410	1.360	1.461	1.408	61.1	0.007

^a In angstroms. ^b In degrees. ^c For crystallographic data for **Class II** donors **OMN** and **MA**, their cation-radicals and nitrosonium complexes (from ref 22), see Tables S2 and S3 in Supplementary Information. ^d Same as in Table 2. ^e Average C–C bond. ^f Angle (in degrees) between O–C bond and arene plane. ^g Increase of average C–C bond in cation radical and complex relative to neutral donor.

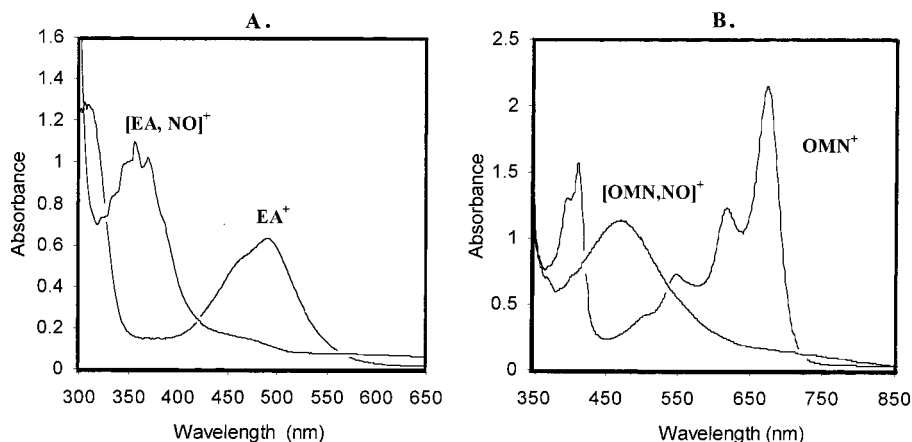


Figure 4. Spectral changes of the **Class II** cation radical to the inner-sphere complex **[ArH,NO⁺]** accompanying the addition of nitric oxide (in excess) in dichloromethane solution: (A) conversion of $\sim 2 \times 10^{-4}$ M **EA⁺** to **[EA,NO⁺]** at 22 °C and (B) conversion of $\sim 2 \times 10^{-4}$ M **OMN⁺** to **[OMN,NO⁺]** at -77 °C. The same spectral changes (in reverse order) are observed upon the removal of nitric oxide (in vacuo) from the inner-sphere complex.

Table 5. Spectral Characteristics of **[ArH,NO⁺]** Complexes from **Class II** Donors^a

donor	E_{ox}^0 (V vs SCE)	λ_{H} , nm [$10^{-3}\epsilon$, $\text{M}^{-1}\text{cm}^{-1}$]	λ_{L}^b , nm	ν_{NO} , cm^{-1}
MA	1.16	360 [8.3]	580	1910
EA	1.30	348 [7.0]	560	1905
OMN	1.34	463 [6.2]	590	1930
DMT	1.43	481 [7.1]	615	1935
TMM	1.45	343 [8.3]	555	^c

^a In dichloromethane at -90 °C. ^b Approximate owing to low intensities of band L and possible overlap by cation-radical bands. ^c Not measured.

donors, with the intense high energy band (H) at $\lambda_{\text{CT}} = 350$ – 500 nm ($\epsilon_{\text{CT}} \approx 8000 \text{ M}^{-1}\text{cm}^{-1}$) and a broad, low-energy band (L) centered at $\lambda_{\text{CT}} = 500$ – 800 nm. It is noteworthy that the polycyclic donors **OMN** and **DMT** were also converted to charge-transfer complexes showing similar spectral characteristics (Figure 4B) as those of other donors, the (vibrational) fine structure in the cation-radical spectrum (Table 3) simply disappearing upon complexation with **NO⁺** (Figure 4B).

The charge-transfer complexes of **Class II** donors uniformly exhibited IR stretching bands with more or less invariant frequencies $\nu_{\text{NO}} = 1905$ – 1935 cm^{-1} that were close to that of free **NO⁺** gas with $\nu_{\text{NO}} = 1876 \text{ cm}^{-1}$.

B. Structural Change Of Class II Donors upon NO⁺ Complexation. Single crystals of the **NO⁺** complexes with **Class II** donors were isolated by the slow diffusion of hexane into a dichloromethane solution at -80 °C. Selected bond distances and bond angles of the various **ArH/NO⁺** associations determined by X-ray crystallographic analysis are listed in

Tables 4 and S3 for comparison with the structural parameters of the corresponding neutral donors (**ArH**) and cation radicals (**ArH⁺**) in Tables 4 and S2. From the latter comparison, we concluded that upon **NO⁺** complexation (i) the aromatic framework undergoes significant expansion to that extant in the cation radical **ArH⁺**, as indicated by the Δ values in Tables 4 and S3, and (ii) the N–O bond distance increases to that in reduced nitric oxide. Otherwise, the structural parameters are quite close to those in the **[HMB,NO⁺]** complex, as representative of the most electron-rich aromatic donor in **Class I** (Tables 2 and S1). Further indication that these **[ArH,NO⁺]** complexes actually consist of the intermolecular association of **ArH⁺** and **NO⁺** is shown in the hydroquinone donor **MA** that affords the complex (Figure 5A) in which both methoxy groups are rotated into the aromatic plane with $\beta = 6.6^\circ$ (relative to $\beta = 72^\circ$ in the uncomplexed donor), and such a coplanarization is the structural change diagnostic of **MA⁺** with $\beta = 2.2^\circ$. It is also noteworthy that **NO⁺** complexation to the naphthalene donor **OMN** occurs on only one ring (Figure 5B), which suffers a large expansion ($\Delta \approx 1.1$ pm) while the uncomplexed ring is relatively unchanged ($\Delta \approx 0.1$ pm). Such an unsymmetrical distribution of bond lengths is indicative of the uneven electron redistribution in the **OMN⁺** moiety^{18,19} resulting from its strong electronic interaction with coordinated nitric oxide. A similar severe polarization of aromatic donors upon **Cr(CO)₃** complexation was previously observed in a series of arene/**Cr(CO)₃** complexes.²²

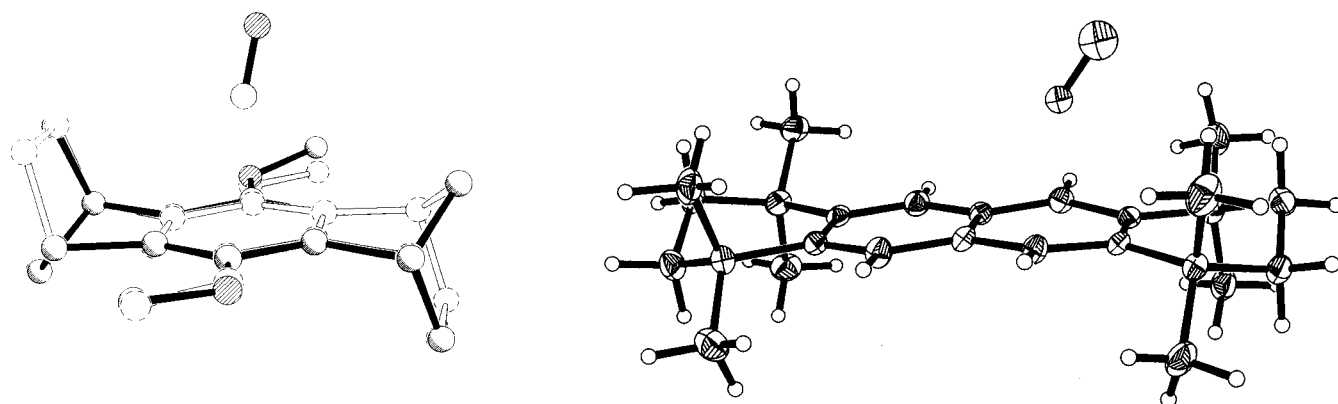


Figure 5. ORTEP diagrams of the NO^+ complexes with **Class II** aromatic donors: (left) hydroquinone ether donor **MA** (black lines) with the structure of the cation radical $\text{MA}^{\bullet+}$ superimposed (open lines) for structural comparison and (right) naphthalene donor **OMN** showing the NO^+ complexation on only one ring.

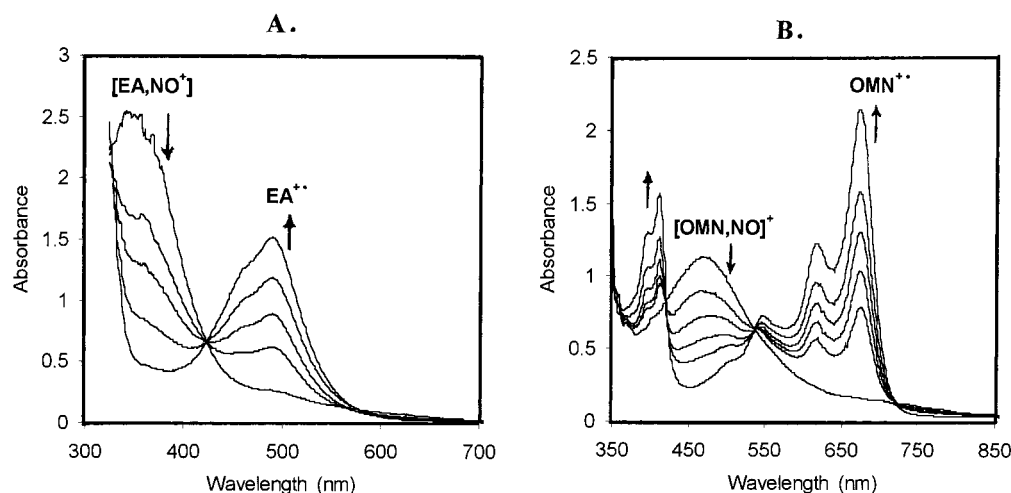
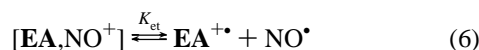


Figure 6. Temperature modulation of the reversible complexation/electron transfer between **Class II** aromatic donors and NO^+ : (A) increase of $\text{EA}^{\bullet+}$ at (bottom to top) -44 , -10 , 3 , and 20 °C and after argon bubbling (to remove NO) and (B) increase of $\text{OMN}^{\bullet+}$ at (bottom to top) -90 , -30 , -10 , 0 , and 20 °C and after argon bubbling.

IV. Temperature Modulation of the Reversible Complexation/Electron Transfer between (Class II) Aromatic Donors and Nitrosonium Cation. The interchange between the aromatic complex $[\text{ArH},\text{NO}^+]$ and the aromatic cation radical $\text{ArH}^{\bullet+}$, as described in eqs 4 and 5, could be carried out reversibly in the following way. Thus the addition of NO^+ to a solution of **EA** contained in a fully filled cuvette (sans vapor space) at 22 °C led to a mixture of both $[\text{EA},\text{NO}^+]$ and $\text{EA}^{\bullet+}$, as shown by the diagnostic bands at $\lambda_{\text{CT}} = 348$ nm and $\lambda_{\text{CR}} = 492$ nm, respectively. When the sealed cuvette was decreasingly cooled to -44 °C, the 492-band of $\text{EA}^{\bullet+}$ gradually disappeared, accompanied by the concomitant increase of the 348-band. Likewise, when the chilled cuvette was increasingly warmed, the 490-band of $\text{EA}^{\bullet+}$ gradually reappeared as the 348-absorbance decreased, as illustrated in Figure 6A. The clean isosbestic point at 420 nm provided clear evidence for the reversible character of the dissociative interchange:



Such spectral changes were completely reproducible over multiple cooling/warming cycles. As argon was carefully bubbled through the dichloromethane solution at room temperature to remove NO^{\bullet} , the 348-band of $[\text{EA},\text{NO}^+]$ began to disappear until only the 492-band of $\text{EA}^{\bullet+}$ remained, whereupon no further spectral change was observed on cooling this solution

to -77 °C. Precisely the same series of temperature-dependent spectral changes was observed (in opposite sequence) when the crystalline cation radical salt $\text{EA}^{\bullet+}\text{SbCl}_6$ was treated with nitric oxide.

The reversible interchange was also readily observed with the polycyclic donors **OMN** and **DMT**. Thus, the treatment of the cation radicals $\text{OMN}^{\bullet+}$ and $\text{DMT}^{\bullet+}$ with highly structured (vibrational) absorption bands in the 500–800 nm region (Figure 3B/Table 3) at low temperature afforded charge-transfer spectra (Figure 6B) with the same general features as those of benzenoid donors, with the exception that the intense high-energy band was red-shifted to $\lambda_{\text{H}} = 460$ and 480 nm, respectively (Table 5). [Quantitative IR spectral analysis of the ArH/NO^+ complexes confirmed the N–O stretching band at $\nu_{\text{NO}} \approx 1910$ cm^{-1} (Table 5) to be characteristically close to that of nitric oxide.] Spectral changes accompanying the reversible interchange in Figure 6B between the $[\text{OMN},\text{NO}^+]$ complex and the $\text{OMN}^{\bullet+}$ cation radical in the temperature range $+20$ to -90 °C was clearly defined by a pair of isosbestic points at 400 and 540 nm.



V. Quantitative Evaluation of the Equilibrium Constants for the Complexation and the Electron-Transfer Steps. The reversible formation of the charge-transfer complex of **ArH** and

Table 6. Equilibrium Constants and Thermodynamics of Electron Transfer and $[\text{ArH},\text{NO}]^+$ Complex Formation for **Class II** Donors^a

donor	K_{CT} (M^{-1})	$-\Delta G_{\text{ET}}$ (kcal M^{-1})	K_{ET}	K_{et} (M)	ΔH_{et} (kcal M^{-1})	ΔS_{et} ($\text{cal M}^{-1} \text{K}^{-1}$)
MA	5.1×10^7	7.3	2.8×10^5	5.5×10^{-3}	8.3	15.0
EA	1.5×10^6	4.1	1.2×10^3	8.2×10^{-4}	12.9	28.6
OMN	3.9×10^5	3.2	2.4×10^2	6.3×10^{-4}	8.3	13.1
DMT	3.0×10^4	1.1	7.1×10^0	2.4×10^{-4}	10.7	20.2
TMM	1.0×10^5	0.7	3.2×10^0	3.2×10^{-5}		

^a In CH_2Cl_2 , at 22 °C.

NO^+ , as delineated by K_{CT} in eq 2, together with its reversible dissociation to $\text{ArH}^{+\bullet}$ and NO^{\bullet} , as delineated by K_{et} in eqs 6 and 7, represent a set of reversible (coupled) equilibria (eq 8)



that is inherent to the *overall* electron-transfer process in eq 1.

For a **Class II** aromatic donor, the equilibrium constant K_{et} was evaluated in Table 6 by the quantitative (multiwavelength) analysis of each composite spectrum (such as those shown in Figure 6 at different temperatures). The concentrations of $\text{ArH}^{+\bullet}$ and $[\text{ArH},\text{NO}^+]$ were based on their spectral characteristics, independently established in Tables 3 and 5, respectively (see Experimental Section for details of the spectral analysis).²³ The thermodynamic parameters were evaluated from the temperature-dependent changes of K_{et} between 22 and -90 °C (see Experimental Section) and are also listed in Table 6.

The values of K_{ET} for overall electron transfer were evaluated from the Nernst relationship of the free-energy change:

$$\Delta G_{\text{ET}} = \mathcal{F} (E^{\circ}_{\text{ox}} - E^{\circ}_{\text{red}}) \quad (9)$$

where E°_{ox} (Table 1) is the oxidation potential of the aromatic donor and $E^{\circ}_{\text{red}} = 1.48$ V vs SCE is the reduction potential of nitrosonium cation in dichloromethane.^{10a} The values of K_{CT} for **Class II** donors obtained from K_{et} and K_{ET} (since $K_{\text{ET}} = K_{\text{et}}K_{\text{CT}}$) are also included in Table 6.

For the **Class I** donors, the absence of persistent cation radicals (*vide supra*) precluded the direct determination of K_{et} . Accordingly, the operation was reversed and the complexation constants K_{CT} were first measured from the prominent charge-transfer spectrum in Table 1 by the Benesi–Hildebrand and Drago procedures.^{13,14} The free-energy change of the overall electron transfer for **Class I** donors was then evaluated by the same procedure as that in eq 9. The (putative) dissociative equilibria (K_{et}) for **Class I** donors were calculated from K_{CT} and K_{ET} as described above, and these are also included in Table 7.²⁴

Discussion

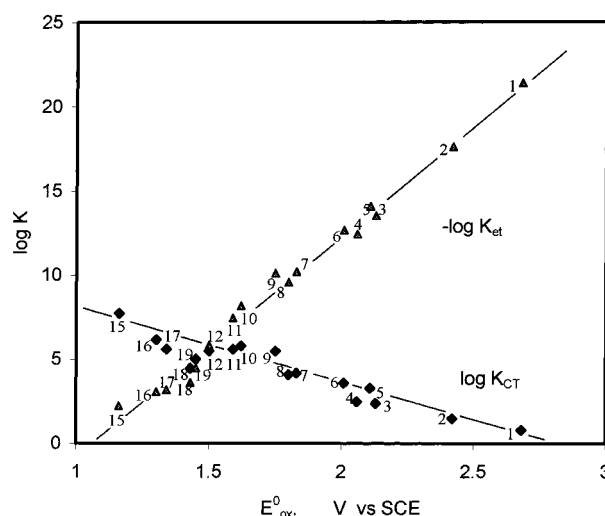
The reversible electron transfer between various aromatic donors and NO^+ (eq 1) proceeds via the inner-sphere complex

(23) The charge-transfer spectra of **Class I** donors with NO^+ were also scrutinized at very low temperatures, but we were unable to observe these aromatic cation radicals.

(24) (a) The equilibrium constant K_{CT} and K_{et} for **Class I** donors were only evaluated at 22 °C since the large magnitude of K_{CT} and the competing formation of 2:1 complexes did not allow us to determine reliable values of the thermodynamic parameters for (1:1) complex formation. (b) Figure 7 shows that the electron-transfer equilibria (eqs 6 and 7) for **Class I** donors fall in the range $6 \leq \log K_{\text{et}} < 23$. Thus, at the lower limit (23), the calculated concentration of (reactive) cation radicals (e.g., $\text{BEN}^{+\bullet} < 10^{-13}$ M) will be too low for significant *bimolecular* reaction to occur within the time scale of our measurements. [For example, all of our measurements were carried out with freshly prepared reagents and made within a period of less than 5 min.] At the upper limit ($-\log K_{\text{et}} = 6$), competition from the analogous bimolecular (kinetics) processes is more favorable (e.g., $\text{HMB}^{+\bullet} \approx 10^{-6}$ M), but the cation radicals derived from these electron-rich donors are also significantly more persistent (see Howell et al. in ref 8a).

Table 7. Equilibrium Constants and Thermodynamics of Electron Transfer and $[\text{ArH},\text{NO}]^+$ Complex Formation for **Class I** Donors^a

donor	ΔG_{ET} (kcal M^{-1})	K_{ET}	K_{et} (M)
BEN	27.4	3.7×10^{-21}	4.0×10^{-22}
TOL	21.5	1.0×10^{-16}	2.3×10^{-18}
<i>o</i> -XY	14.9	8.6×10^{-12}	2.8×10^{-14}
<i>p</i> -XY	13.3	1.3×10^{-10}	3.5×10^{-13}
MES	14.4	1.9×10^{-11}	7.7×10^{-15}
TBB	12.1	9.5×10^{-10}	2.0×10^{-13}
DUR	8.0	1.1×10^{-6}	6.21×10^{-11}
TPB	7.3	3.6×10^{-6}	2.6×10^{-10}
PMB	6.2	2.5×10^{-5}	7.3×10^{-11}
HMB	3.2	4.1×10^{-3}	6.3×10^{-9}
HEB	2.5	1.3×10^{-2}	3.3×10^{-8}
TMT	0.5	4.6×10^{-1}	1.4×10^{-6}

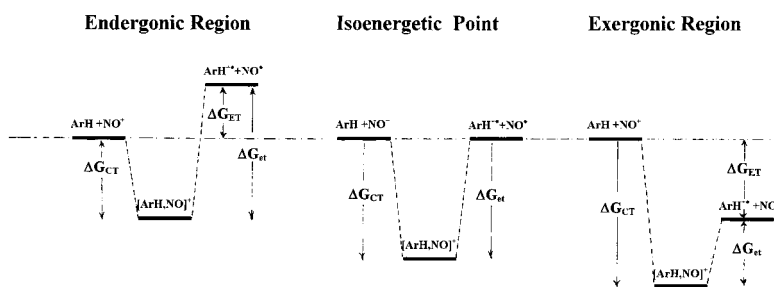
^a In CH_2Cl_2 , at 22 °C.**Figure 7.** Linear dependence of the equilibrium constants for complexation ($\log K_{\text{CT}}$) and electron transfer ($-\log K_{\text{et}}$) on the oxidation potential (E°_{ox}) of **Class I** and **Class II** aromatic donors.

$[\text{ArH},\text{NO}^+]$ as the *obligatory* intermediate established in eq 8. As such, the pair of coupled equilibria involving (a) the diffusive formation of $[\text{ArH},\text{NO}^+]$ from ArH plus NO^+ and (b) its subsequent dissociative separation into the product $\text{ArH}^{+\bullet}$ plus NO^{\bullet} , as given by K_{CT} and K_{et} , respectively, relate directly to the overall electron-transfer process (K_{ET}).

I. Critical Role of the Inner-Sphere Complex to the Electron-Transfer Process. A. Linear Correlation of K_{CT} and K_{et} with the Driving Force for Electron Transfer. The structural effects of the aromatic donor (ArH) on the K_{CT} and K_{et} steps can be evaluated separately by their dependence on the driving force ($-\Delta G_{\text{ET}}$) for electron transfer. As such, Figure 7 illustrates the unmistakable *linear* dependence of the associative (preequilibrium) step ($\log K_{\text{CT}}$) as well as dissociative equilibrium ($-\log K_{\text{et}}$)²⁵ on the electron-transfer driving force, which is given simply by the oxidation potential (E°_{ox}) of the

(25) The reciprocal of the dissociative equilibrium constant is plotted in Figure 7 as $-\log K_{\text{et}}$ in order to key in on the energy of the inner-sphere complex relative to that of the ion-radical pair (and not vice versa).

Chart 3



various arenes (since the acceptor strength of NO^+ is a nonvariable). It is particularly noteworthy that the **Class I** and **Class II** arene donors (as disparate as they are) both fall precisely on a single linear correlation. In other words, the transitory cation radicals of a **Class I** donor and the persistent cation radicals of a **Class II** donor are *indistinguishable* insofar as their effect on either $\log K_{\text{CT}}$ or $-\log K_{\text{et}}$ is concerned. In both cases, the remarkable linear correlations of $\log K_{\text{CT}}$ and $-\log K_{\text{et}}$ that cover a span of more than 35 kcal mol^{-1} in the electron-transfer driving force include all aromatic donors in a pair of linear free-energy relationships (LFER) readily expressed as

$$\log K_{\text{CT}} = -aE_{\text{ox}}^{\circ} + \text{const} \quad (10)$$

$$-\log K_{\text{et}} = bE_{\text{ox}}^{\circ} + \text{const} \quad (11)$$

where $a = 4.3$ and $b = 13$. The negative slope for the associative LFER indicates that the stabilization of the $[\text{ArH}, \text{NO}^+]$ complex increases with donor strength, and the same is true for the dissociative step, which progressively increases in importance with donor strength. [The magnitude of the (absolute) ratio $|a/b|$ indicates that complexation ($\log K_{\text{CT}}$) is roughly 3 times more sensitive to structural changes in the aromatic donor than that in the dissociative step ($-\log K_{\text{et}}$) leading to the (separated) ion-radical pair.] The crossover point of the two linear correlations in Figure 7 occurs at $E_{\text{ox}}^{\circ} = 1.48 \text{ V}$, where the two equilibria are comparable (i.e., $\log K_{\text{CT}} = -\log K_{\text{et}}$) and corresponds to the isoenergetic point for the overall electron transfer with $K_{\text{ET}} = 1$. The latter also indicates that the isoenergetic point must correspond to the donor strength of the reduced nitric oxide, which in fact has an independently measured value of $E_{\text{ox}}^{\circ} = 1.48 \text{ V}$ vs SCE in dichloromethane.¹⁰

B. Free-Energy Changes in the Formation of Inner-Sphere Complexes. The importance of the inner-sphere complex relative to the reactant and product states can be evaluated directly as the free-energy changes for the associative (K_{CT}) and dissociative (K_{et}) steps. Since the relative energies of the reactant state ($\text{ArH} + \text{NO}^+$) and the product state ($\text{ArH}^{\bullet+} + \text{NO}^{\bullet}$) are determined solely by the aromatic donor strength, there are three (potential) regions with $E_{\text{ox}}^{\circ}(\text{ArH})$ greater than, equal to, or less than $E_{\text{ox}}^{\circ}(\text{NO}^{\bullet})$ that correspond to the endergonic region, isoenergetic point, and exergonic region, respectively, of the electron-transfer driving force ($-\Delta G_{\text{ET}}$). In the endergonic region, the equilibrium occurs mainly between the inner-sphere complex and the reactant state consisting of uncomplexed NO^+ and ArH . Conversely, in the exergonic region, the equilibrium depends mainly on the inner-sphere complex and the product state composed of the separated ion-radical pair $\text{ArH}^{\bullet+}$ and NO^{\bullet} , as graphically illustrated by the free-energy changes along the (idealized) reaction coordinate in Chart 3.

Accordingly, let us consider the function ΔG_{IS} as the free-energy difference between the inner-sphere complex from its

closest nonassociated state. Thus, inspection of Chart 3 indicates that for the endergonic region with $E_{\text{ox}}^{\circ} > 1.5 \text{ V}$, the inner-sphere complex predominates and $\Delta G_{\text{IS}} = \Delta G_{\text{CT}}$, whereas in the exergonic region with $E_{\text{ox}}^{\circ} < 1.5 \text{ V}$, the ion-radical pair predominates and $\Delta G_{\text{IS}} = \Delta G_{\text{et}}$. At the isoenergetic potential, $\Delta G_{\text{IS}} = \Delta G_{\text{CT}} = \Delta G_{\text{et}}$. The general function of ΔG_{IS} is expressed as

$$\Delta G_{\text{IS}} = \frac{\Delta G_{\text{CT}} + \Delta G_{\text{et}} + |\Delta G_{\text{ET}}|}{2} \quad (12)$$

(the derivation of which is given in the Experimental Section). The plot of ΔG_{IS} against the electron-transfer driving force in Figure 8A clearly establishes the maximum stabilization of the inner-sphere complex to occur at the isoenergetic potential.

C. Populations of the Inner-Sphere Complex with Changes in the Driving Force. The foregoing conclusion also derives from a view of the inner-sphere complex as its distribution among the various particles extant in the K_{CT} and K_{et} equilibria. Accordingly, we consider the population of the inner-sphere complex relative to the sum of all nonassociated (uncomplexed) species as

$$\alpha = \frac{[\text{ArH}, \text{NO}^+]}{[\text{ArH} + \text{NO}^+ + \text{ArH}^{\bullet+} + \text{NO}^{\bullet}]} \quad (13)$$

The graphical representation of the population ratio α as a function of E_{ox}° is illustrated in Figure 8B at two extreme (initial) concentrations (C_0) of ArH and NO^+ [see Experimental Section for the analytical expression of α vs E_{ox}° and C_0]. The maximum population of the inner-sphere complex clearly appears in Figure 8B again at close to the isoenergetic potential.

II. MO Formulation of the Inner-Sphere Complex. The energetics and populations consideration in Figure 8A and B confirm the stability and the concentration of the inner-sphere complex to maximize at the isoenergetic potential. Furthermore, X-ray crystallographic analysis (Tables 2, 4, S1, and S3) indicate that the NO binding to the aromatic chromophore occurs at distance (2.1 \AA) that is substantially less than the van der Waals separation of 3.25 \AA to reflect the pronounced inner-sphere character of the $[\text{ArH}, \text{NO}^+]$ complexes. Coupled with the accompanying enlargement of the aromatic moiety upon complexation (see Tables 2, 4, S1, and S3), we now inquire as to the nature of the NO binding to the aromatic donor that induces such dramatic structural changes in the donor/acceptor pair.

A. LCAO-MO Formulation of the Inner-Sphere Complex. To describe the inner-sphere complex quantitatively, we proceed from the mutual interaction of the donor/acceptor molecular orbitals according to basic LCAO methodology,²⁶ in which only the frontier orbitals of ArH (HOMO) and NO^+ (LUMO) are explicitly taken into account.²⁷ The accompanying (simplified) orbital diagram²⁸ for the donor/acceptor interaction of benzene (ArH) and NO^+ is presented below, in which the linear

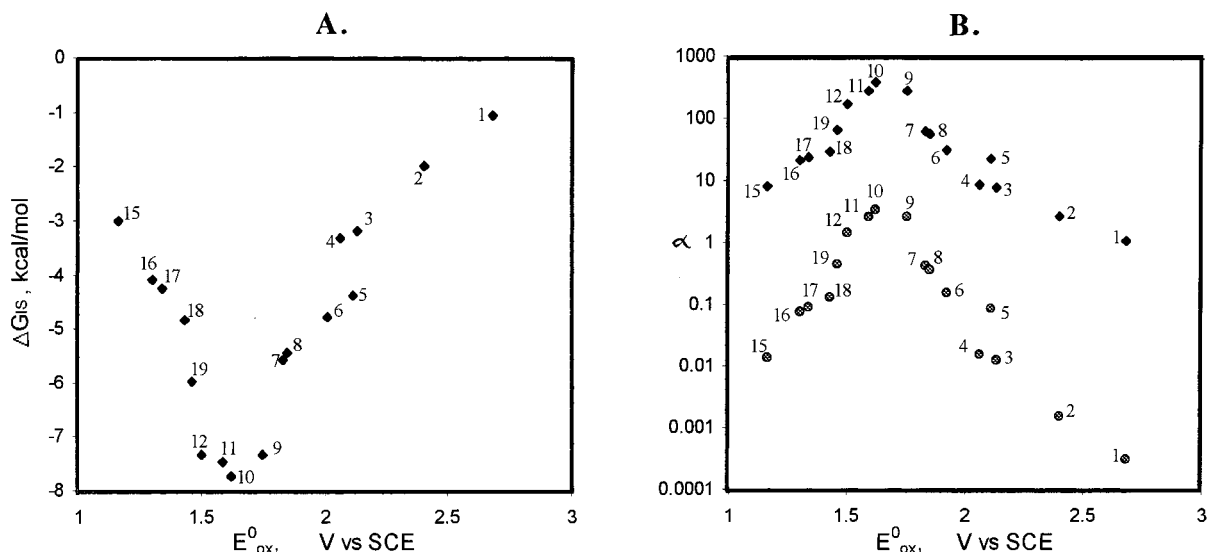


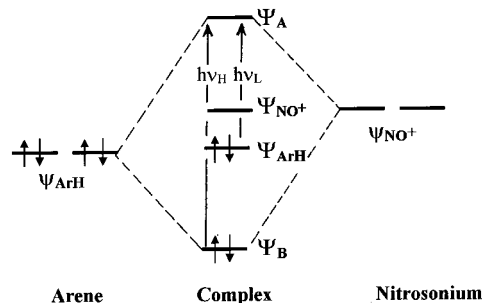
Figure 8. Nonlinear variation of (A) the free-energy difference (ΔG_{\ddagger} in eq 12) and (B) population (α in eq 13) of the inner-sphere complex with changes in the electron-transfer driving force. The numbers identify both **Class I** and **Class II** aromatic donors in Tables 1 and 3. Note in (B) at **ArH** concentrations of 1 M (top) and 10^{-4} M (bottom).

combination of donor/acceptor orbitals leads to a new bonding orbital $\Psi_B = C_{\text{NO}}\psi_{\text{NO}} + C_{\text{ArH}}\psi_{\text{ArH}}$ and a new antibonding orbital $\Psi_A = C'_{\text{NO}}\psi_{\text{NO}} + C'_{\text{ArH}}\psi_{\text{ArH}}$ of the inner-sphere complex. The coefficients are normalized so that

$$C_{\text{NO}}^2 + C_{\text{ArH}}^2 = 1 \quad \text{and} \quad C'_{\text{NO}}^2 + C'_{\text{ArH}}^2 = 1 \quad (14)$$

According to Chart 4, the absorption spectra of the inner-sphere complexes (Tables 1 and 5) are assigned to a pair of electronic transitions from (i) the bonding MO (Ψ_B) to the antibonding MO (Ψ_A) and (ii) the nonbonding MO (Ψ_{ArH}) to the antibonding MO (Ψ_A) of the inner-sphere complex, as designated by $h\nu_{\text{H}}$ (high-energy band) and $h\nu_{\text{L}}$ (low-energy band), respectively. Although both electronic transitions are

Chart 4



allowed, the limited overlap of Ψ_{ArH} with Ψ_A will result in an appreciably less intense low-energy band.

Application of the standard variation method²⁹ leads to the energies of the new (bonding and antibonding) molecular orbitals as³⁰

$$\epsilon_B = \frac{(\epsilon_{\text{NO}} + \epsilon_{\text{ArH}}) - (\Delta_{\text{AB}}^2 + 4H_{\text{AB}}^2)^{1/2}}{2} \quad (15)$$

$$\epsilon_A = \frac{(\epsilon_{\text{NO}} + \epsilon_{\text{ArH}}) + (\Delta_{\text{AB}}^2 + 4H_{\text{AB}}^2)^{1/2}}{2} \quad (16)$$

where the coulomb integrals ($\epsilon_i = \int \psi_i H \psi_i$) represent electron energies of the constituent donor and acceptor orbitals, and the resonance integral ($H_{\text{AB}} = \int \psi_{\text{NO}} H \psi_{\text{ArH}}$) represents the donor/acceptor electronic interaction energy in the inner-sphere complex.

Since the HOMO–LUMO gap is given by $\Delta_{\text{AB}} = \epsilon_{\text{NO}} - \epsilon_{\text{ArH}}$, we evaluate it experimentally (in solution) as the driving force for the overall electron-transfer process, i.e.,³¹

(29) For a detailed discussion of the variation method, see for example: (a) Epstein, S. T. *The Variation Method in Quantum Chemistry*; Academic Press: New York, 1974. (b) Streitwieser, A. J. *Molecular Orbital Theory for Organic Chemists*; Wiley: New York, 1961.

(30) (a) The same expressions for ϵ_B and ϵ_A as well as the low- and high-energy transitions were obtained by the linear combination of the reactant and the (redox) product states by (b) Creutz, C.; Newton, M. D.; Sutin, N. J. *Photochem. Photobiol. A: Chem.* **1994**, *82*, 47. Compare also the expressions for $h\nu_{\text{L}}$ and $h\nu_{\text{H}}$ by (c) Zwickel, A. M.; Creutz, C. *Inorg. Chem.* **1971**, *10*, 2395.

(26) (a) Hückel, E. *Grundzüge der Theorie ungesättigter and aromatischer Verbindungen*; Verlag Chemie, G.m.b.H.: Berlin, 1938. (b) Flurry, R. L., Jr. *Molecular Orbital Theories of Bonding in Organic Molecules*; Marcel Dekker: New York, 1968. (c) Jorgensen, W. L.; Salem, L. *The Organic Chemist's Book of Orbitals*; Academic Press: New York, 1973. Dewar, M. J. S.; Dougherty, R. C. *The PMO Theory of Organic Chemistry*. Plenum Press: New York, 1975 (e) Carroll, F. A. *Perspectives on Structure and Mechanism in Organic Chemistry*; Brooks/Cole Publishing Company: New York, 1998 For the application of MO-LCAO methodology to charge-transfer complexes, see: (f) Flurry, R. L. *J. Phys. Chem.* **1965**, *69*, 1927. (g) Flurry, R. L. *J. Phys. Chem.* **1969**, *73*, 2111. (h) Flurry, R. L. *J. Phys. Chem.* **1969**, *69*, 2787. Note that Flurry's approach cannot be used for calculation of MO energetics of the complexes under study, since he considered the extent of charge transfer to be constant in the series of complexes.

(27) (a) Fleming, I. *Frontier Orbitals and Organic Chemical Reactions*; Wiley: New York, 1976. (b) Traven, V. F. *Frontier Orbitals and Properties of Organic Molecules*; Ellis Horwood: New York, 1992. (c) Klopman, G. *J. Am. Chem. Soc.* **1968**, *90*, 223. (d) Fukui, K. *Acc. Chem. Res.* **1971**, *4*, 57. (e) Fukui, K. *Angew. Chem., Int. Ed. Engl.* **1982**, *21*, 801.

(28) (a) Compare Rauk, A. *Orbital Interaction Theory of Organic Chemistry*; Wiley: New York, 1994. Note, however, our spectral assignments differ. In Rauk's assignment, the high-energy band corresponds to $\Psi_{\text{ArH}} \rightarrow \Psi_A$, which is inconsistent with the experimental results (vide infra). Furthermore, Rauk's assignment of the low energy band is also at variance with the experimental results, since the experimental transition energy ($h\nu_{\text{L}} = 2.5\text{--}3\text{ eV}$) differs substantially from the HOMO–LUMO gap ($<1.5\text{ eV}$). We did not take into account the LUMO of benzene because of its much higher energy compared to the NO^+ LUMO and benzene HOMO [compare electron affinities of -1.15 eV (BEN^\ominus) and $+9.26\text{ eV}$ (NO^+)^{1a}; reduction potentials, -3.2 V (BEN^\ominus)^{1a} and $+1.48\text{ V}$ (NO^+)¹⁰]. (b) Alternatively, the low-energy band can be assigned to the transition $\Psi_B \rightarrow \Psi_{\text{NO}^+}$, but it leads to no change in the discussion on the intensity and the expression for the energy of $h\nu_{\text{L}}$ (vide infra eq 19); (c) Jordan, K. D.; Burrow, P. D. *Acc. Chem. Res.* **1978**, *11*, 341.

$$\Delta_{AB} \cong E_{\text{ox}}^{\circ}(\text{ArH}) - E_{\text{red}}^{\circ}(\text{NO}^+) \quad (17)$$

The resonance integral H_{AB} can be obtained with the aid of eqs 15 and 16 by recognizing the high-energy band ($h\nu_{\text{H}}$) to derive from the transition $\Psi_{\text{B}} \rightarrow \Psi_{\text{A}}$, i.e.,³²

$$h\nu_{\text{H}} = \epsilon_{\text{A}} - \epsilon_{\text{B}} = (\Delta_{\text{AB}}^2 + 4H_{\text{AB}}^2)^{1/2} \quad (18)$$

The Δ_{AB} values in eq 17 and H_{AB} values in eq 18 were calculated from the spectral data ($h\nu_{\text{H}}$) and E_{ox}° potentials listed in Tables 1 and 5, and they are tabulated in Table 8 for both **Class I** and **Class II** aromatic donors.

B. Experimental Verification of the MO Method for Inner-Sphere Complexes. To test the validity of the assignment in eqs 17 and 18, we apply two independent criteria as follows.

(1) *The Mulliken correlation of the (low-energy) charge-transfer band.* According to Chart 3, the low-energy band corresponds to the electronic transition $\Psi_{\text{ArH}} \rightarrow \Psi_{\text{A}}$, and the energy of the transition $h\nu_{\text{L}} = \epsilon_{\text{A}} - \epsilon_{\text{ArH}}$ can be directly evaluated from eq 16 as

$$h\nu_{\text{L}} = \frac{(\Delta_{\text{AB}}^2 + 4H_{\text{AB}}^2)^{1/2}}{2} + \frac{\Delta_{\text{AB}}}{2} \quad (19)$$

The experimental (low-energy) spectrum ($h\nu_{\text{L}}$ in Table 1) is compared with the calculated spectrum (eq 19 and Table 8) in Figure 9A. The solid line represents the least squares treatment of all the spectral data and has a slope of 1.02 with the correlation coefficient 0.94 to confirm the validity of the simplified MO method to correctly account for the electronic changes in the inner-sphere complexes.³³

(2) *Degree of charge transfer in inner-sphere complexes.* The characteristic feature of the inner-sphere complexes is their variable (X-ray) structures (Tables 2 and 4), which are also obvious from the spectral variation of the N–O stretching frequencies (ν_{NO} in Table 1) with donor strength. Both measures reflect changes in the degree of charge transfer (hereinafter designated as **Z**) from the aromatic donor to the NO^+ acceptor (see section IC in Results). Since the acceptor is a simple diatomic, the changes in ν_{NO} represent an unambiguous (experimental) measure of **Z**, i.e.,¹¹

$$\mathbf{Z} = \frac{\nu_{\text{NO}^+}^2 - \nu_{\text{IS}}^2}{\nu_{\text{NO}^+}^2 - \nu_{\text{NO}}^2} \quad (20)$$

where subscript NO^+ represents the (uncomplexed) nitrosonium cation, IS the inner-sphere complex, and NO the (completely) reduced nitric oxide.

Theoretically, the degree of charge transfer can be viewed as the excess charge residing on the NO^+ moiety in the inner-sphere complex. For the bonding MO (Ψ_{B}) such an excess is evaluated as $2C_{\text{NO}^+}$ (eq 14).²⁶ The values of $2C_{\text{NO}^+}$ obtained by the variation method²⁹ are plotted against the experimental **Z** values in Figure 9B. The unmistakable linear correlation again confirms the validity of the MO method to correctly predict the diagnostic changes in degree of charge transfer with the aromatic donor strength. Moreover, the absolute magnitude of $2C_{\text{NO}^+}$ is remarkably close to the experimental **Z**, especially for the most electron-rich members of **Class I** donors.³⁴

III. Electronic Nature of the Donor/Acceptor Binding in the Inner-Sphere Complex. Since the $[\text{ArH}, \text{NO}^+]$ complex is central to the electron-transfer process in eq 8, let us examine the electronic factors leading to its stabilization in the context of the MO framework. According to Chart 4, the energy gain during the complex formation is assigned to the difference in the electronic (orbital) energy: $\Delta E \cong \epsilon_{\text{ArH}} - \epsilon_{\text{B}}$, because electron (charge) transfer from the arene to the complex orbital (see Chart 4, Tables 2, 4, S1, S3, and Figure 9B) plays a large role in the stabilization.³⁵ Such an energy gain is expressed (with the aid of eq 15) as

$$\Delta E \cong \frac{(\Delta_{\text{AB}}^2 + 4H_{\text{AB}}^2)^{1/2}}{2} - \frac{\Delta_{\text{AB}}}{2} \quad (21)$$

To evaluate ΔE (eq 21), we note that the dependence of the resonance (exchange) integral H_{AB} (Table 8) on the aromatic

(34) (a) Figure 10 includes only the endergonic region of the driving force since we are unable to evaluate **Z** in the exergonic region (owing to an inappropriate eq 20). Note that despite a nearly complete electron transfer from ArH to NO^+ , various ArH/ NO^+ associations are completely esr silent. (b) The highest deviation is observed with the weakest donors, which may possibly be connected to the largest electrostatic effects in such complexes.³³

(35) Other factors that can influence the stabilization of inner-sphere complexes such as solvation, entropy, etc, appear to be constant (see Flurry in refs 26f–h).

(31) The electron energy in a particular (localized) orbital is usually characterized in the gas phase by its ionization potential. However, the energies of the frontier orbitals in solution are best approximated by the redox potentials. For the discussion of this point, see refs 27b and 8a.

(32) The H_{AB} values can be also calculated from the Mulliken–Hush equation (see, e.g., ref 30b) using the spectral band maximum (ν), the bandwidth ($\Delta\nu_{1/2}$), the extinction coefficient (ϵ), and the donor/acceptor separation (d_{AB}), so that $H_{\text{ab}} = 2.06 \times 10^{-2} \times (\nu \times \epsilon \times \Delta\nu_{1/2})^{1/2} / d_{\text{AB}}$. The values calculated in this way for inner-sphere complexes lie in the 1.0–1.5 eV range, and their dependence on the arene redox potential and steric hindrance is similar to those obtained via eq 18. However, the latter afforded a much better agreement of the calculated values of the degree of charge transfer with the experimental **Z** and are thus used below.

(33) (a) Note that the experimental points lie consistently higher (~ 0.45 eV) than the calculated points. The shortfall may be attributed to the less than optimal Frank–Condon factor and/or by an extraneous influence of electrostatic interactions [in which the energy of the noninteracting arenes orbital are lowered due to the positive charge on the arene]. The electrostatic factor was not explicitly taken into account in the calculation of MO energetics since any electrostatic interaction of a positively charge acceptor and neutral donor would increase the energy of both bonding and antibonding orbitals by similar amounts.^{26c} As a result, the electrostatics will not affect the calculation of H_{AB} based on the $\epsilon_{\text{B}}/\epsilon_{\text{A}}$ difference, but it will be important in the calculations of the absolute values of $h\nu_{\text{L}}$, the extent of charge transfer (**Z**), and the stabilization energy (E) of the inner-sphere complex. (b) We wish to reemphasize that the LCAO–MO treatment given here also theoretically predicts that the Mulliken correlation for the high-energy band (experimentally observed in Figure 1C) will show little if any slope. See footnote 36.

Table 8. Values of Δ_{AB} and H_{AB} for **Class I** and **Class II** Donors^a

donor	Δ_{AB} (V)	H_{AB} (eV)	donor	Δ_{AB} (V)	H_{AB} (eV)	donor	Δ_{AB} (V)	H_{AB} (eV)
BEN	1.22	1.74	TMT	0.02	1.79	DTB	0.55	1.82
TOL	0.94	1.77	TET	0.07	1.79	MTB	0.66	1.77
o-XY	0.65	1.82	ODM	0.22	1.88	OME	0.41	1.85
p-XY	0.58	1.85	MA	-0.32	1.72	EME	0.51	1.82
MES	0.63	1.80	EA	-0.18	1.80	TIP	0.51	1.81
TBB	0.53	1.80	OMN	-0.14	1.34	MDU	0.45	1.89
DUR	0.35	1.87	DMT	-0.05	1.29	ODU	0.44	1.89
TPB	0.32	1.82	TMM	-0.03	1.82	OMO	0.45	1.85
PMB	0.27	1.86	ETB	0.79	1.78	DMA	0.12	1.84
HMB	0.14	1.87	CUM	0.81	1.78	MME	0.10	1.87
HEB	0.11	1.83	TBU	0.84	1.76			

^a Based on electrochemical and spectral data in dichloromethane from Tables 1, 5, and S4 (see Supplementary Information) (notation: **ETB**, ethylbenzene; **CUM**, cumene; **TBU**, *tert*-butylbenzene; **DTB**, 1,4-ditertbutylbenzene; **MTB**, 1,3-ditertbutylbenzene; **OME**, 1,3,4-trimethylbenzene; **EME**, 1,3,5-triethylbenzene; **TIP**, 1,3,5-triisopropylbenzene; **MDU**, 1,2,3,5-tetramethylbenzene; **ODU**, 1,2,3,4-tetramethylbenzene; **OMA**, 1,1,4,4,5,5,8,8-octamethyl-1,2,3,4,5,6,7,8-octahydroanthracene; **DMA**, 1,2,3,4,5,6,7,8-octahydro-1,4:5,8-dimethanoanthracene; **MME**, 5,6,7,8-tetramethyl-1,2,3,4-tetrahydro-1,4-ethanonaphthalene.

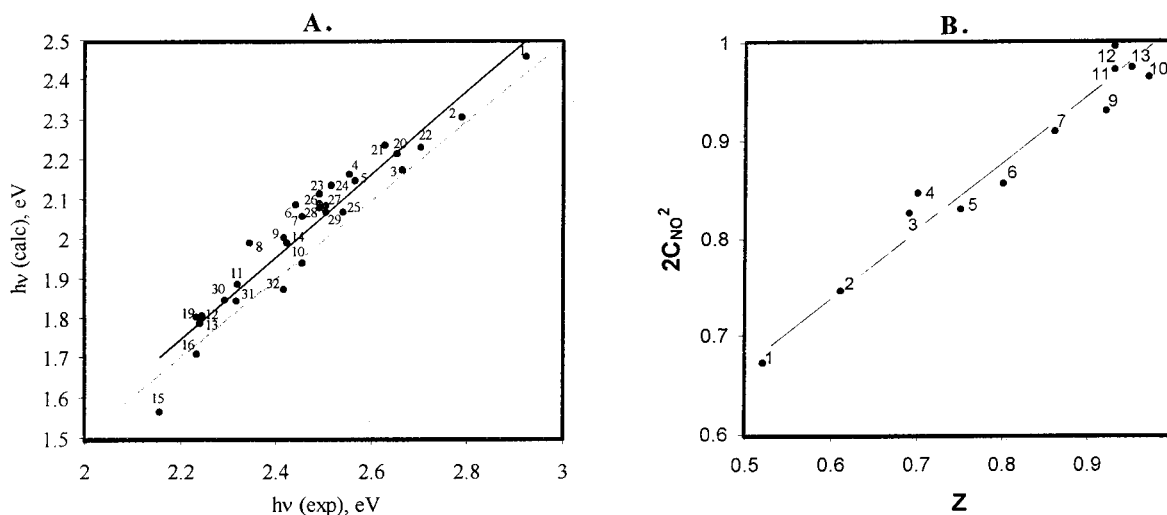


Figure 9. Verification of the MO method for inner-sphere complexes showing the direct (linear) relationship between the experimental (abscissa) and the calculated (A) transition energy ($h\nu_L$) for the Mulliken correlation of the low-energy bands of arene donors identified in Tables 1, 3, and 10 for both **Class I** and **Class II** donors and (B) populations ($2C_{NO^2}$) of the inner-sphere complex for **Class I** donors. Note that the dashed line in 9A is arbitrarily drawn with a unit slope to emphasize the validation.

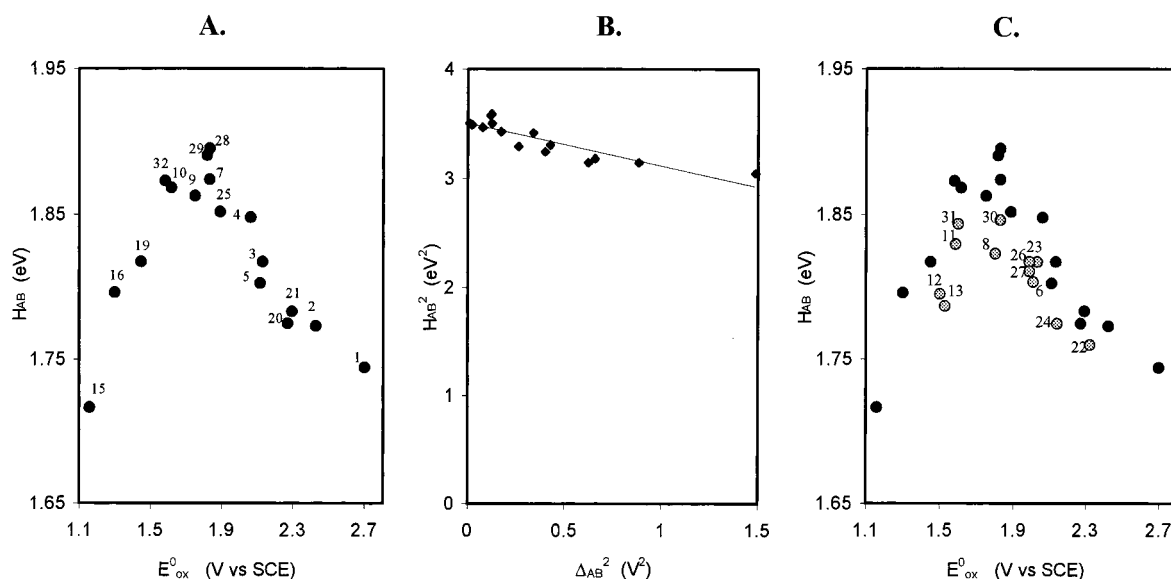


Figure 10. Mechanistic significance of the electronic coupling element as shown by (A) maximum value of H_{AB} at the isoenergetic point to reflect the optimum stability of the inner-sphere complex, (B) the compensating effects of H_{AB} and the driving-force function Δ_{AB} for its relation to ΔG_{IS} , and (C) the reduction of H_{AB} in sterically hindered donors (identified as grey circles). Numbers identify both **Class I** and **Class II** donors in Tables 1, 3, and 10.

donor strength (illustrated in Figure 10A) shows a maximum at the isoenergetic potential $E^{\circ}_{ox} = 1.5$ V, and the application of eq 17 suggests, that H_{AB}^2 decreases as Δ_{AB}^2 increases. The compensating effect of H_{AB}^2 and Δ_{AB}^2 is illustrated in Figure 10B, and we thus conclude that the first term in eq 21 is nearly constant.³⁶ As a result, the energy gain ΔE for complex formation in eq 21 will change linearly with Δ_{AB} , and this conclusion is verified by the experimental LFER expressed in eq 10 and illustrated in Figure 7 as the linear correlation of $\log K_{CT}$ and E°_{ox} .

(36) It is particularly noteworthy that the compensation of Δ_{AB}^2 by H_{AB}^2 is also revealed in the UV-vis spectra in Figure 1C. Thus, according to Chart 3 the high-energy band (as given by eq 18) will result from the offsetting effects of Δ_{AB}^2 and H_{AB}^2 and will show no (or little) dependence on the aromatic donor strength (compare the upper experimental spectra in Figure 1C). On the other hand, the low-energy band expressed by eq 19 will be linearly dependent on E°_{ox} (compare the lower spectra in Figure 1C (Mulliken correlation)).

The stabilization energy in eq 21 basically consists of two components: (i) the bonding/antibonding (orbital) splitting given by $\epsilon_A - \epsilon_B$ in eq 18, and (ii) the HOMO - LUMO gap Δ_{AB} in eq 17. Inspection of the relative values of H_{AB} and Δ_{AB} (listed in Table 8) reveals the inequality: $4H_{AB}^2 \gg \Delta_{AB}^2$ (except in the endergonic limits). If so, this approximation, as applied to eq 21, leads to the qualitative conclusion that ΔE and H_{AB} are strongly coupled. In other words, the stabilization energy of complex formation is largely determined by the donor/acceptor electronic interaction energy $H_{AB} = \int \psi_{NO} H \psi_{AH}$. Such a conclusion predicts that the electronic exchange (H_{AB}) between the donor and acceptor orbitals in the inner-sphere complex plays a major role in the experimental free-energy change (ΔG_{IS}), as indeed confirmed by the strong similarity of their energy dependencies shown in Figures 10A and 8A, respectively. In both cases, maximum stabilization occurs at the isoenergetic potential, and the attainment of maximum values of H_{AB}

coincides with the optimal interaction of the interacting orbitals with matched energies³⁷ (compare Chart 3).

The effectiveness of such an orbital overlap can also be adversely affected by any steric hindrance in the aromatic donors that inhibits the approach of the NO⁺ acceptor. In our study, such an encumbrance is induced by annelation (as in compounds **12**, **13**, **30**, and **31**) or by a bulky group in the benzenoid donor (see Tables 1 and S4), and the steric effect is observed in Figure 10C by a H_{AB} value that is significantly less than that of their unhindered analogue. A further correlation of H_{AB} values with structural characteristics of the inner-sphere complex is not apparent at this juncture. For example, the intermolecular ArH–NO separation for the weak donors (**BEN** and **TOL**) is somewhat larger (2.75 and 2.66 Å)³⁸ than that (2.1 Å) in other complexes (Table 2), but they are unfortunately not in the form of 1:1 complexes. Furthermore, maximal H_{AB} values appear at the tilt angle $\alpha = 140^\circ$, but this dependence is not reliably so.

IV. Mechanistic Relevance of the Inner-Sphere Complex to Electron-Transfer Theories. The dominant role of the inner-sphere complex as the key intermediate in the electron-transfer process between aromatic donors and nitrosonium cation must be considered in the theoretical light of Marcus–Hush theory.^{39,40} However, the sizable magnitude of the resonance (exchange) integral H_{AB} in Table 8 clearly excludes the outer-sphere mechanism for electron transfer in which the electronic coupling element between ArH and NO⁺ must be restricted to 200 cm⁻¹. Accordingly, we now turn to Sutin's development of the Marcus–Hush formulation that specifically includes electronic coupling elements > 200 cm⁻¹.⁴¹ In particular, Sutin considers two additional major mechanistic categories in which the limits of the electronic coupling element are (i) $H_{AB} > 200$ cm⁻¹ but less than $\lambda/2$ and (ii) $H_{AB} > \lambda/2$, where λ is the Marcus reorganization energy. These mechanistic categories correspond to the classic Robin-Day classification⁴² of mixed-valence complexes: *Class I* with $H_{AB} = 0$, *Class II* with $0 < H_{AB} < \lambda/2$, and *Class III* with $H_{AB} > \lambda/2$. In other words, as the magnitude of H_{AB} increases, the barrier for electron transfer decreases progressively, and at the limit of large H_{AB} , the donor/acceptor system is completely delocalized. Since the magnitude of H_{AB} is directly related to the kinetics barrier, *Class II* complexes with $H_{AB} \leq 200$ cm⁻¹ correspond to the Marcus outer-sphere mechanism for electron transfer. By default, electron-transfer systems with $H_{AB} \geq 200$ cm⁻¹ are considered to proceed via inner-sphere mechanisms.⁴³

(37) (a) For such an optimum orbital interaction, see ref 27a,b. (b) It is particularly noteworthy that the hindered polycyclic aromatic donors **OMN** and **DMT** are characterized by H_{AB} values (1.34 and 1.28 eV) that are offscale.

(38) A number of imprecise (partially disordered) X-ray structural data for the ArH/NO⁺ associations of methylbenzenes are available; see: (a) Brownstein, S.; Gabe, E.; Lee, F.; Tan, L. *J. Chem. Soc., Chem. Commun.* **1984**, 1566. (b) Brownstein, S.; Gabe, E.; Lee, F.; Piotrowski, A. *Can. J. Chem.* **1986**, *64*, 1661. (c) Brownstein, S.; Gabe, E.; Louie, B.; Piotrowski, A. *Can. J. Chem.* **1987**, *65*, 1661. (d) Kim, E. K.; Kochi, J. K. *J. Org. Chem.* **1993**, *58*, 786 and references therein.

(39) (a) Marcus, R. A. *J. Chem. Phys.* **1957**, *26*, 867. (b) Marcus, R. A. *Discuss. Faraday Soc.* **1960**, *29*, 21. (c) Marcus, R. A. *J. Phys. Chem.* **1963**, *67*, 853. (d) Marcus, R. A. *J. Chem. Phys.* **1965**, *43*, 679.

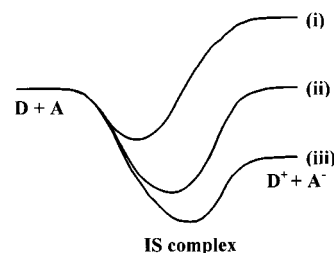
(40) (a) Hush, N. S. *Z. Electrochem.* **1957**, *61*, 734. (b) Hush, N. S. *Trans. Faraday Soc.* **1961**, *57*, 557. (c) Hush, N. S. *Prog. Inorg. Chem.* **1967**, *8*, 391. (d) Hush, N. S. *Electrochim. Acta* **1968**, *13*, 1005.

(41) Sutin, N. *Prog. Inorg. Chem.* **1983**, *30*, 441. See also: Sutin, N. *Adv. Chem. Phys.* **1999**, *106*, 7. Brunschwig, B. S.; Sutin, N. *Coord. Chem. Rev.* **1999**, *187*, 233.

(42) Robin, M. B.; Day, P. *Adv. Inorg. Chem. Radiochem.* **1967**, *10*, 247.

(43) Kochi, J. K. *Angew. Chem., Int. Ed. Engl.* **1988**, *27*, 1227. See also Ebersson et al. in ref 3 and Hubig et al. in ref 4.

Chart 5



To place the ArH/NO⁺ redox system within this context, we estimate the reorganization energy of the cross reaction as $\lambda = 50\text{--}60$ kcal mol⁻¹ (2.4–2.6 eV) from the reported reorganization energy of aromatic donors and the nitrosonium acceptor with $\lambda_{ArH} = 40\text{--}50$ kcal mol⁻¹ and $\lambda_{NO} = 70$ kcal mol⁻¹.¹ Since the values of H_{AB} in Table 8 exceed $\lambda/2 = 1.2\text{--}1.3$ eV, the inner-sphere complex belongs to the Robin-Day *Class III* category, and it is properly designated as [ArH,NO]⁺, with the charge placed *outside* the brackets to emphasize the existence of only one potential minimum on the pathway between the ArH + NO⁺ reactants and the ArH^{•+} + NO[•] products.⁴⁴

Intermolecular electron-transfer reactions that belong to the *Class III* category must occur with no activation energy. Chart 5 qualitatively depicts the free-energy change along the reaction coordinate for the redox transformation of such a donor (D)/acceptor (A) pair for the (i) endergonic, (ii) isergonic, and (iii) exergonic regions.

In each case, no energy barrier separates D and A from the electron-transfer product D⁺ and A⁻ (and vice versa). Such a conclusion is indeed verified by high level quantum mechanical calculations by Skokov and Wheeler⁴⁵ who showed that the charge-transfer (inner-sphere) complex between benzene and NO⁺ is formed without a significant barrier.⁴⁵ As such, electron transfer is not a kinetics process but is dependent on the thermodynamics in which electron redistribution is concurrent with complex formation. Chart 5 emphasizes the inner-sphere (IS) complex to take on maximum significance at the isoenergetic potential (compare the experimental results in Figure 8). Accordingly, we have drawn the free-energy diagram for the endergonic and exergonic processes to reflect the relative positions of the inner-sphere complex along the reaction coordinate. As such, we believe that the diagrams in Chart 5 represent the experimental/theoretical support to the merging of kinetics and thermodynamics concepts, as insightfully adumbrated in the Hammond postulate.⁴⁶

Experimental Section

Materials. Nitrosonium hexachloroantimonate was prepared from SbCl₅ and NOCl according to the literature procedure.¹¹ The alkylbenzenes (Aldrich) were purified by repeated recrystallization from ethanol

(44) (a) In this formulation, the traditional precursor and successor complexes have limited kinetics significance. (b) Note that the high degree of charge transfer in this inner-sphere complex differs from the usual weak (charge-transfer) complexes treated by Mulliken theory. Accordingly, the high-energy band cannot truly be described as a charge-transfer band, and we prefer to describe it in the term of a bonding–antibonding transition, which is confirmed by the insensitivity of $h\nu_H$ of the solvent polarity (see ref 11). (d) The implications to the photochemical activation of [ArH,NO⁺] complexes⁴⁵ will be reported separately. (e) We believe that the changeover from *Class III* to *Class II* complexes will provide additional insight into the mechanism of the inner-sphere electron-transfer, and structural factors that affect (lower) H_{AB} are now under study. (f) Hubig, S. M.; Kochi, J. K. *J. Am. Chem. Soc.* **2000**, *122*, 8279. (g) Bockman, T. M.; Karpinski, Z. J.; Sankaraman, S.; Kochi, J. K. *J. Am. Chem. Soc.* **1992**, *114*, 1920.

(45) Skokov, S.; Wheeler, R. A. *J. Phys. Chem A* **1999**, *103*, 4261.

(46) Hammond, G. S. *J. Am. Chem. Soc.* **1955**, *77*, 534.

or fractional distillation. The synthesis of trimethanododecahydrotriphenylene (TMT),¹⁷ triethanododecahydrotriphenylene (TET),¹⁷ 9,10-dimethoxy-1,4:5,8-dimethano-1,2,3,4,5,6,7,8-octahydroanthracene²⁰ (MA), 9,10-ethoxy-1,4:5,8-diethano-1,2,3,4,5,6,7,8-octahydroanthracene (EA),²⁰ dimetoxidurene (TMM),⁶ the cyclo-annulated naphthalene (1,1,4,4,7,7,10,10-octamethyl-1,2,3,4,7,8,9,10-octahydronaphthalene (OMN)),⁹ 5,6,7,8-tetramethyl-1,2,3,4-tetrahydro-1,4-ethanonaphthalene (MME),¹⁷ and triphenylene (1,1,4,4,7,7,10,10,13,13,16,16-dodecamethyl-1,2,3,4,7,8,9,10,13,14,15,16-dodecahydronaphthoanthracene (DMT)),¹⁵ 1,1,4,4,5,5,8,8-octamethyl-1,2,3,4,5,6,7,8-octahydroanthracene (OMA),⁶ 1,2,3,4,5,6,7,8-octahydro-1,4:5,8-dimethanoanthracene (DMA)⁶ were described previously. Dichloromethane (Merck), hexane (Merck), and acetonitrile (Merck) were purified according to standard laboratory procedures⁴⁹ and were stored in Schlenk flasks under an argon atmosphere. Nitric oxide (C.P., Matheson) was purified by passing it through a column filled with KOH pellets.⁴⁹

Instrumentation. The UV-vis absorption spectra were recorded on a HP 8453 diode-array spectrometer. The ¹H and ¹³C NMR spectra were obtained on a General Electric QE-300 FT NMR spectrometer. Infrared (IR) spectra were recorded on a Nicolet 10D FT spectrometer. Electrochemical apparatus and the procedure for the determination of the oxidation potentials have been described elsewhere.⁴⁷ All operations were performed in an inert atmosphere box in a Teflon-capped cuvettes equipped with a sidearm.

General Procedure for the Preparation of Cation-Radical Salt. A 50-mL flask fitted with a quartz cuvette and a Schlenk adaptor was charged with nitrosonium salt (0.2 mmol), and a solution of the hydroquinone ether MA (54 mg, 0.2 mmol) in anhydrous dichloromethane was added under an argon atmosphere at 25 °C. UV-vis spectral analysis of NO revealed the characteristic absorptions at λ_{\max} = 204, 214, and 226 nm,⁴⁸ and it was removed by entrainment with a stream of argon. The red-orange solution was stirred (while slowly bubbling argon through the solution) for 15 min to yield a dark-red solution of cation radical [MA⁺SbCl₆⁻]. Spectrophotometric analysis of the highly colored solution indicated the quantitative formation of [MA⁺SbCl₆⁻]. The deep-red solution was carefully layered with dry toluene (30 mL) and placed in a refrigerator (-23 °C). In the course of 3 days, bright-red crystals of the cation-radical salts were deposited. The similar procedure was employed for the preparation of other cation radical salts in Table 4.

General Procedure for the Preparation of Inner-Sphere Complexes [ArH,NO]⁺. A 50-mL flask fitted with a Schlenk adapter was charged with nitrosonium salt (0.2 mmol), and a solution of the aromatic donor (0.2 mmol) in anhydrous dichloromethane was added under an argon atmosphere (for Class II donors at -77 °C). The deep-red solutions were layered with dry hexane (30 mL) and placed in a -77 °C bath. During the course of 3–5 days, dark brown-red crystals of the complex [ArH,NO]⁺SbCl₆⁻ were deposited.

Preparation of the Crystals of the Cationic Salt of ODM. A 50-mL flask fitted with a quartz cuvette and a Schlenk adapter was charged with nitrosonium salt (0.2 mmol), and a solution of the aromatic donor (0.2 mmol) in anhydrous dichloromethane was added under an argon atmosphere at 22 °C. The solution was kept in the dark for ~4 h at room temperature to complete the redox transformation (as monitored by UV-vis spectra). Then solution was carefully layered with hexane and placed in a -77 °C bath, and dark red crystals formed during 3 days.

X-ray Crystallography. The intensity data for all of the compounds were collected with the a Siemens SMART diffractometer equipped with a 1K CCD detector using Mo K α radiation (λ = 0.71073 Å) at -150 °C. The structures were solved by direct methods⁵¹ and refined by full matrix least-squares procedure with IBM Pentium and SGI O2

computers. [Note that the X-ray structure details of various compounds mentioned here are on deposit and can be obtained from Cambridge Crystallographic Data Center, U.K.]

[*p*-XY,NO⁺]SbCl₆⁻. Brutto formula C₈H₁₀Cl₆NOSb. MW = 470.62. Monoclinic *P*₂/*m*, *a* = 7.9010(2), *b* = 9.3692(3), *c* = 10.5385(3) Å, β = 97.836(1)°, *V* = 3759.36(4) Å³, *D*_c = 2.022 g cm⁻³, *Z* = 2. The total number of reflections measured were 9724 of which 3700 reflections were symmetrically nonequivalent. Final residuals were *R*₁ = 0.0268 and *wR*₂ = 0.0583 for 3155 reflections with *I* > 2 σ (*I*).

[*o*-XY,NO⁺]SbCl₆⁻·1/2CH₂Cl₂. Brutto formula: C_{8.5}H₁₁Cl₇NOSb. Monoclinic *C*2/*c*, *a* = 15.8869(2), *b* = 26.333(1), *c* = 11.2138(6) Å, β = 131.578(1)°, *V* = 3509.3(3) Å³, *D*_c = 1.942 g cm⁻³, *Z* = 8. The total number of reflections measured were 22395 of which 7713 reflections were symmetrically nonequivalent. Final residuals were *R*₁ = 0.0398 and *wR*₂ = 0.0836 for 5454 reflections with *I* > 2 σ (*I*).

[DUR,NO⁺]SbCl₆⁻. Brutto formula: C₁₀H₁₄Cl₆NOSb. MW = 498.67. Monoclinic *P*₂/*c*, *a* = 15.8110(8), *b* = 10.6325(5), *c* = 11.2600(6) Å, β = 109.154(1)°, *V* = 1788.1(2) Å³, *D*_c = 1.852 g cm⁻³, *Z* = 4. The total number of reflections measured were 14991, of which 7311 reflections were symmetrically nonequivalent. Final residuals were *R*₁ = 0.0269 and *wR*₂ = 0.0650 for 5004 reflections with *I* > 2 σ (*I*).

[PMB,NO⁺]SbCl₆⁻. Brutto formula: C₁₁H₁₆Cl₆NOSb. MW = 512.70. Orthorhombic *Pbcm* (structure disordered through crystallographic mirror plane), *a* = 8.0136(5), *b* = 19.1586(7), *c* = 12.2616(11) Å, *V* = 1882.5(2) Å³, *D*_c = 1.809 g cm⁻³, *Z* = 4. The total number of reflections measured were 26356, of which 4363 reflections were symmetrically nonequivalent. Final residuals were *R*₁ = 0.0408 and *wR*₂ = 0.1117 for 3397 reflections with *I* > 2 σ (*I*).

EA. Brutto formula: C₂₂H₃₀O₂. MW = 326.46. Monoclinic *P*₂/*c*, *a* = 9.5633(4), *b* = 10.2163(4), *c* = 10.0282(4) Å, β = 111.230(1)°, *V* = 913.28(6) Å³, *D*_c = 1.187 g cm⁻³, *Z* = 2. The total number of reflections measured were 11137, of which 3993 reflections were symmetrically nonequivalent. Final residuals were *R*₁ = 0.0505 and *wR*₂ = 0.1190 for 2904 reflections with *I* > 2 σ (*I*).

EA⁺SbCl₆⁻. Brutto formula: C₂₂H₃₀O₂Cl₆Sb. MW = 660.91. Monoclinic *P*₂/*n*, *a* = 10.1384(1), *b* = 16.2556(1), *c* = 15.9955(2) Å, β = 92.921(1)°, *V* = 2632.73(4) Å³, *D*_c = 1.667 g cm⁻³, *Z* = 4. The total number of reflections measured were 33007, of which 11908 reflections were symmetrically nonequivalent. Final residuals were *R*₁ = 0.0412 and *wR*₂ = 0.0805 for 9072 reflections with *I* > 2 σ (*I*).

[EA,NO⁺]SbCl₆⁻. Brutto formula: C₂₂H₃₀O₂Cl₆NOSb. MW = 690.92. Triclinic *P*-1, *a* = 10.0424(4), *b* = 15.1279(1), *c* = 19.3211(8) Å, α = 69.4888(3), β = 83.497(3)°, γ = 80.602(3)°, *V* = 2707.3(2) Å³, *D*_c = 1.695 g cm⁻³, *Z* = 4. The total number of reflections measured were 33977, of which 23344 reflections were symmetrically nonequivalent. Final residuals were *R*₁ = 0.0529 and *wR*₂ = 0.0777 for 13595 reflections with *I* > 2 σ (*I*).

Measurement of the Charge-Transfer Spectra of Inner-Sphere Complexes of Class I Donors with Nitrosonium. The spectral data in Table 1 were typically measured at [NOSbCl₆]₀ = 0.5–1.0 mM and [ArH] = 0.5–20 mM in 0.1–1.0-cm quartz cuvettes at 22 °C under an argon atmosphere. To obtain the energy of the bands H and L, the UV-vis spectra were deconvoluted into Gaussian components. Table S4 includes charge-transfer data for the various (additional) alkylated benzenes used in this study.

Determination of *K*_{CT} and ϵ _{CT} for Nitrosonium Complexes with Class I Arenes. For relatively weak donors (BEN to MES), the aliquots of standard stock (dichloromethane) solutions of NOSbCl₆ and arenes were transferred to a 1-cm quartz cuvette (the concentrations of NO⁺ were 0.2–2.0 mM and of arene, 0.5–20 mM). The absorbances (*A*_{CT}) of the solutions were measured at 340 nm (band H). On the basis of spectral data for different ArH/NO⁺ ratios, the equilibrium constants *K*_{CT} and extinction coefficient ϵ _{CT} were calculated using the graphical methods of Drago based on dependence of *K*_{CT}⁻¹ against ϵ _{CT}¹⁴ and by Benesi-Hildebrand procedure, based on [NO⁺]/*A*_{CT} versus [ArH]⁻¹.¹³

For electron-rich Class I donors, linear dependencies of the *A*_{CT} on the concentration of arene were observed (see Supplementary), when the concentrations were in range NO⁺ = 0.5–1.0 mM and ArH = 0.1–0.5 mM. Under these conditions, electron-rich donors are completely associated as the inner-sphere complex. Thus, [ArH,NO]⁺ = [ArH]₀ and ϵ _{CT} for different electron-rich arene were calculated directly

(47) Rathore, R.; Bosch, E.; Kochi, J. K. *Tetrahedron* **1994**, *32*, 2620.

(48) Bosch, E.; Rathore, R.; Kochi, J. K. *J. Org. Chem.* **1994**, *59*, 2529.

(49) (a) Perrin, D. D.; Armarego, W. L. F.; Perrin, D. R. *Purification of Laboratory Chemicals*, 2nd ed.; Pergamon: New York, 1980. (b) Shriver, D. F.; Drezdson, M. A. *The Manipulation of Air-sensitive Compounds*, 2nd ed.; Wiley: New York, 1986.

(50) Note that the oxidation potential of hydroquinone ether MA was rather insensitive to temperature changes and increased by only 50 mV upon decreasing the temperature from +25 to -50 °C in dichloromethane.

(51) Sheldrick, G. M. *SHELXS-86, Program for Structure Solution*; University of Göttingen: Germany, 1986.

from A_{CT} . The values of ϵ_{CT} were checked by measuring the absorbance of solutions containing a large excess of arene (where $[\text{ArH}, \text{NO}^+] = [\text{NOSbCl}_6]_0$). To determine K_{CT} , the absorbance A_{CT} of the solutions containing substantially lower concentrations of reagents $[\text{NO}^+ = 0.05\text{--}0.2\text{ mM}$ and $\text{ArH} = 0.01\text{--}0.2\text{ mM}]$ were measured. Under these conditions, an appreciable fraction of the reagents remained uncomplexed and allowed us to calculate K_{CT} according to the relationship $K_{CT} = [\text{ArH}, \text{NO}^+]/([\text{ArH}]_0 - [\text{ArH}, \text{NO}^+])([\text{NOSbCl}_6]_0 - [\text{ArH}, \text{NO}^+])$, where $[\text{ArH}, \text{NO}^+] = A_{CT}/\epsilon_{CT}$, the equilibrium concentration of the complex, and $[\text{ArH}]_0$ and $[\text{NOSbCl}_6]_0$ are the initial concentrations of the arenes and nitrosonium cation, respectively.

Determination of K_{et} for Class II Donors. The addition of NO^+ to a dichloromethane solution of a **Class II** donor contained in a fully filled cuvette at 22 °C led to a mixture of both $[\text{ArH}, \text{NO}^+]$ and $\text{ArH}^{+\bullet}$, as shown by their diagnostic UV–vis absorption bands. Since the UV–vis (300–1000 nm) absorption of the solution derives from the sum of cation radical and the complex, the absorbance at a given wavelength (A^λ) can be expressed as (a) $A^\lambda = [\text{ArH}, \text{NO}^+]\epsilon_c^\lambda + [\text{ArH}^{+\bullet}]\epsilon_r^\lambda$, where ϵ_c^λ and ϵ_r^λ are the extinction coefficients of $[\text{ArH}, \text{NO}^+]$ and $\text{ArH}^{+\bullet}$ at wavelength λ . For the solutions with $[\text{NO}^+]_0 = 0.1\text{--}0.3\text{ mM}$ and $[\text{ArH}]_0 = 0.5\text{--}2\text{ mM}$, the following equalities are valid at equilibrium, viz., (i) $[\text{ArH}^{+\bullet}] = [\text{NO}^*]$ (owing to the conservation of charge) and (ii) $[\text{NO}] + [\text{ArH}, \text{NO}^+] = [\text{NO}^+]_0$ owing to $[\text{NO}^*] \approx 0$ at $[\text{NO}^+]_0 < [\text{ArH}]_0$. Therefore, the equilibrium constant K_{et} (eq 6, see Results) can be expressed as (b) $K_{et} = [\text{ArH}^{+\bullet}][\text{NO}^*]/[\text{ArH}, \text{NO}^+] = [\text{ArH}^{+\bullet}]^2/([\text{NO}^+]_0 - [\text{ArH}^{+\bullet}])$. From (b), the concentration of $[\text{ArH}^{+\bullet}]$ can be written as (c) $[\text{ArH}^{+\bullet}] = \{(1 + 4[\text{NO}^+]_0/K_{et})^{1/2} - 1\}K_{et}/2$. By taking into account equality (ii), the absorbance at wavelength λ is expressed as (d) $A^\lambda = ([\text{NO}^+]_0 - [\text{ArH}^{+\bullet}])\epsilon_c^\lambda + [\text{ArH}^{+\bullet}]\epsilon_r^\lambda = [\text{NO}^+]_0\epsilon_c^\lambda + [\text{ArH}^{+\bullet}](\epsilon_r^\lambda - \epsilon_c^\lambda)$. From eqs c and d, A^λ is expressed via K_{et} and known values of $[\text{NO}^+]_0$, ϵ_c^λ , and ϵ_r^λ , that is, (e) $A^\lambda = [\text{NO}^+]_0\epsilon_c^\lambda + (\epsilon_r^\lambda - \epsilon_c^\lambda)(1 + 4[\text{NO}^+]_0/K_{et})^{1/2} - 1\}K_{et}/2$. Thus, K_{et} is determined by minimizing the sum of squares of differences between A^λ_{exp} and A^λ , as in (f) $\Delta = \sum (A^\lambda_{\text{exp}} - A^\lambda)^2$, where A^λ_{exp} are absorbances measured at several λ , and A^λ are values calculated for such λ with eq e based on the known values of $[\text{NO}^+]_0$, ϵ_c^λ , and ϵ_r^λ (and the varied K). The calculations of K_{et} are illustrated in the Supporting Information.

The solution was cooled to -90 °C , and the UV–vis absorption spectra were recorded at several intermediate temperatures. The band intensity of the cation radicals progressively decreased upon lowering the temperatures, and it was accompanied by a concomitant increase in the absorbance due to the $[\text{ArH}, \text{NO}^+]$ complex. Accordingly, the appreciable decrease of the dissociation constant of complex (K_{et}) (calculated in accordance with the procedure above) was observed. On the basis of K_{et} values determined at different temperatures, the thermodynamic parameters ΔH_{et} and ΔS_{et} (see Table 6) were calculated from the dependence of $\log K_{et}$ on T^{-1} . The values of K_{et} , ΔH_{et} , and ΔS_{et} for other **Class II** donors presented in Table 6 were calculated by a similar procedure (see Supplementary Information for dependence of $\log K_{et}$ on T^{-1}). The values of Δ at minimum in all cases were less than 0.01, indicating that the experimentally obtained spectra can be appropriately described within this framework.⁵⁰

Calculation of the Equilibrium Ratio α of the Inner-Sphere Complex in Solution. Let us consider, for simplicity, the case where equal initial concentration, C_0 , of $[\text{ArH}]$ and $[\text{NO}^+]$ were taken. Denoting equilibrium concentration of $[\text{NO}^+]$ as C , we can express the equilibrium concentrations of the arene and the complex in solution as (i) $[\text{ArH}] = [\text{NO}^+] = C$ and (ii) $[\text{ArH}, \text{NO}^+] = K_{CT}[\text{ArH}][\text{NO}^+] = K_{CT}C^2$. Since (iii) $[\text{ArH}^{+\bullet}] = [\text{NO}^*]$ and (iv) $K_{ET} = ([\text{ArH}^{+\bullet}][\text{NO}^*])/([\text{ArH}][\text{NO}^+]) = \exp(-\Delta G_{ET}/RT) = K_{CT}K_{et}$, the equilibrium concentration of $\text{ArH}^{+\bullet}$ and NO^* can be expressed as (vi) $[\text{ArH}^{+\bullet}] = [\text{NO}^*] = C \exp(-\Delta G_{ET}/2RT)$. Taking into account eqs i, ii, and vi, the ratio of the equilibrium concentrations of complex to the sum of concentrations of uncomplexed species can be rewritten as $\alpha = [\text{ArH}, \text{NO}^+]/([\text{ArH}] + [\text{NO}^+] + [\text{ArH}^{+\bullet}] + [\text{NO}^*]) = K_{CT}C^2/(2C + 2C \exp(-\Delta G_{ET}/2RT)) = 1/2 K_{CT}C/(1 + \exp(-\Delta G_{ET}/2RT))$. From the $C_0 = ([\text{ArH}, \text{NO}^+] + [\text{NO}^+] + [\text{NO}]) = K_{CT}C^2 + C + C \exp(-\Delta G_{ET}/2RT)$ (material balance for nitrosonium), the equilibrium concentration C can be expressed through the initial concentration C_0 as $C = \{-[1 + \exp(-\Delta G_{ET}/2RT)] + [(1 + \exp(-\Delta G_{ET}/2RT))^2 + 4K_{CT}C_0]^{1/2}\}/2K_{CT}$.

Therefore, α is expressed via C_0 and the equilibrium constants K_{CT} as

$$\alpha = \frac{-\left[1 + \exp\left(\frac{-\Delta G_{ET}}{2RT}\right)\right] + \left[\left(1 + \exp\left(\frac{-\Delta G_{ET}}{2RT}\right)\right)^2 + 4K_{CT}C_0\right]^{1/2}}{4\left[1 + \exp\left(\frac{-\Delta G_{ET}}{2RT}\right)\right]} = \frac{\left[1 + \frac{4K_{CT}C_0}{\left(1 + \exp\left(\frac{-\mathcal{F}(E^\circ_{\text{ox}}(\text{ArH}) - E^\circ_{\text{red}}(\text{NO}^+))\right)}\right)^2}\right]^{1/2} - 1}{4}$$

The values of α calculated with this equation for different donors (based on the K_{CT} and E°_{ox} from Tables 1, 6, and S4) are presented in Figure 8B.

Derivation the Expression for ΔG_{IS} . The free-energy difference between the energy of the complex state and its *closest* nonassociated state (as seen from Chart 3) for the endergonic region equals $\Delta G_{IS} = \Delta G_{CT} = \Delta G_{et} + |\Delta G_{ET}|$ [Note that ΔG_{IS} , ΔG_{CT} , and ΔG_{et} are negative values, while the absolute value of ΔG_{ET} ($|\Delta G_{ET}|$) is positive]. Therefore this free-energy difference can be expressed as $\Delta G_{IS} = [\Delta G_{CT} + \Delta G_{et} + |\Delta G_{ET}|]/2$. In the exergonic region $\Delta G_{IS} = \Delta G_{et} = \Delta G_{CT} + |\Delta G_{ET}|$, and again $\Delta G_{IS} = [\Delta G_{et} + \Delta G_{CT} + |\Delta G_{ET}|]$. Therefore, ΔG_{IS} can be expressed by the same eq 12 in all driving-force regions (at isoenergetic point $\Delta G_{CT} = \Delta G_{et}$ and $|\Delta G_{ET}| = 0$, so thus eq 12 is also correct).

MO Formulation for Inner-Sphere Complexes. According to the simplified MO consideration, as applied to intermolecular interactions, the molecular orbitals of complex (Ψ), can be expressed as the linear combination of the frontier orbitals of the reacting species, i.e., the arene HOMO and the LUMO of NO^+ : $\Psi = C_{\text{NO}}\psi_{\text{NO}} + C_{\text{ArH}}\psi_{\text{ArH}}$. The energy of this orbital is given as (a) $\epsilon = \int \Psi H^{\text{eff}} \Psi / \int \Psi^2 = (C_{\text{NO}}^2 H_{\text{NO}} + C_{\text{ArH}}^2 H_{\text{ArH}} + 2C_{\text{NO}}C_{\text{ArH}}H_{\text{ab}})/(C_{\text{NO}}^2 + C_{\text{ArH}}^2 + 2C_{\text{NO}}C_{\text{ArH}}S_{\text{ab}})$. In this expression, $H_{\text{NO}} = \int \psi_{\text{NO}} H^{\text{eff}} \psi_{\text{NO}} = \epsilon_{\text{NO}}$ and $H_{\text{ArH}} = \int \psi_{\text{ArH}} H^{\text{eff}} \psi_{\text{ArH}} = \epsilon_{\text{ArH}}$ are the energies of the electron localized on the NO and arene, respectively, $H_{\text{ab}} = \int \psi_{\text{NO}} H^{\text{eff}} \psi_{\text{ArH}}$ is the interaction (exchange) integral, and $S_{\text{ab}} = \int \psi_{\text{NO}} \psi_{\text{ArH}}$ is the overlap integral. The wave functions are normalized, i.e., $S_{\text{NO}} = \int \psi_{\text{NO}}^2 = 1$ and $S_{\text{ArH}} = \int \psi_{\text{ArH}}^2 = 1$. The minimum energy solution is found by the variation method, i.e., eq a is differentiated with respect to C_{NO} and C_{ArH} , and the extrema are identified (derivatives equal zero). It leads to system of the two equations (b) $(\epsilon_{\text{NO}} - \epsilon)C_{\text{NO}} + (H_{\text{ab}} - S_{\text{ab}}\epsilon)C_{\text{ArH}} = 0$ and (c) $(H_{\text{ab}} - S_{\text{ab}}\epsilon)C_{\text{NO}} + (\epsilon_{\text{ArH}} - \epsilon)C_{\text{ArH}} = 0$. A solution of the secular determinant for this system results in (d): $(1 - S_{\text{ab}}^2)\epsilon^2 + (2H_{\text{ab}}S_{\text{ab}} - (\epsilon_{\text{NO}} + \epsilon_{\text{ArH}}))\epsilon + \epsilon_{\text{NO}}\epsilon_{\text{ArH}} - H_{\text{ab}}^2 = 0$. From eq d (assuming $S_{\text{ab}} = 0$), the energy of the MOs will be (e) $\epsilon = 1/2((\epsilon_{\text{NO}} + \epsilon_{\text{ArH}}) \pm ((\epsilon_{\text{NO}} - \epsilon_{\text{ArH}})^2 + 4H_{\text{ab}}^2)^{1/2})$ [plus and minus correspond to upper and lower states (antibonding and bonding orbitals of the complex) with energy ϵ_A and ϵ_B]. The energy differences between them is $\epsilon_A - \epsilon_B = (\Delta_{\text{AB}}^2 + 4H_{\text{ab}}^2)^{1/2}$ ($\epsilon_{\text{NO}} - \epsilon_{\text{ArH}}$ is denoted as Δ_{AB}). From eqs b and c, we find C_{NO} and C_{ArH} and therefore C_{NO}^2 and C_{ArH}^2 (which are the probabilities of the electron to reside on the NO and arene, respectively) as $C_{\text{NO}}/C_{\text{ArH}} = H_{\text{ab}}/(\epsilon_{\text{NO}} - \epsilon)$. Taking into account eq e and normalization ($C_{\text{NO}}^2 + C_{\text{ArH}}^2 = 1$), C_{NO}^2 can be expressed as $C_{\text{NO}}^2 = H_{\text{ab}}^2/\{H_{\text{ab}}^2 + 1/4(\Delta_{\text{AB}}^2 + (\Delta_{\text{AB}}^2 + 4H_{\text{ab}}^2)^{1/2})^2\}$ (plus corresponds to bonding and minus to antibonding orbitals). Since H_{ab} values are calculated from the UV–vis spectral data ($h\nu_{\text{H}} = \epsilon_A - \epsilon_B$), it is convenient to express the coefficients directly through the experimental values. Thus, for the bonding orbital, $C_{\text{NO}}^2 = (h\nu_{\text{H}} - \Delta_{\text{AB}})/(2h\nu_{\text{H}})$. [Note that for antibonding orbital $C_{\text{NO}}^2 = (h\nu_{\text{H}} + \Delta_{\text{AB}})/(2h\nu_{\text{H}}) = 1 - (C_{\text{NO}})^2$].

Acknowledgment. We thank Dr. S. V. Lindeman for crystallographic assistance, Dr. R. Rathore for carrying out the initial studies,²¹ and the R.A. Welch Foundation and National Science Foundation for financial support.

Supporting Information Available: Procedure for the calculations of K_{et} , Figures S1–S3, Tables S1–S5, and X-ray crystallographic structure of the diarylmethyl cation from ODM oxidation. (PDF) This material is available free of charge via the Internet at <http://pubs.acs.org>.